





PRMT1 promotes the tumor suppressor function of p14^{ARF} and is indicative for pancreatic cancer prognosis

Antje Repenning^{1,†}, Daniela Happel^{1,†}, Caroline Bouchard¹, Marion Meixner¹, Yesim Verel-Yilmaz², Hartmann Raifer^{3,4}, Lena Holembowski¹, Eberhard Krause⁵, Elisabeth Kremmer⁶, Regina Feederle⁷ , Corinna U Keber⁸, Michael Lohoff⁴, Emily P Slater², Detlef K Bartsch² & Uta-Maria Bauer^{1,*} 

Abstract

The p14^{ARF} protein is a well-known regulator of p53-dependent and p53-independent tumor-suppressive activities. In unstressed cells, p14^{ARF} is predominantly sequestered in the nucleoli, bound to its nucleolar interaction partner NPM. Upon genotoxic stress, p14^{ARF} undergoes an immediate redistribution to the nucleolar and cytoplasm, where it promotes activation of cell cycle arrest and apoptosis. Here, we identify p14^{ARF} as a novel interaction partner and substrate of PRMT1 (protein arginine methyltransferase 1). PRMT1 methylates several arginine residues in the C-terminal nuclear/nucleolar localization sequence (NLS/NoLS) of p14^{ARF}. In the absence of cellular stress, these arginines are crucial for nucleolar localization of p14^{ARF}. Genotoxic stress causes augmented interaction between PRMT1 and p14^{ARF}, accompanied by arginine methylation of p14^{ARF}. PRMT1-dependent NLS/NoLS methylation promotes the release of p14^{ARF} from NPM and nucleolar sequestration, subsequently leading to p53-independent apoptosis. This PRMT1-p14^{ARF} cooperation is cancer-relevant and indicative for PDAC (pancreatic ductal adenocarcinoma) prognosis and chemotherapy response of pancreatic tumor cells. Our data reveal that PRMT1-mediated arginine methylation is an important trigger for p14^{ARF}'s stress-induced tumor-suppressive function.

Keywords apoptosis; arginine methylation; pancreatic cancer; post-translational modification; tumor suppression

Subject Categories Autophagy & Cell Death; Cell Cycle; Post-translational Modifications & Proteolysis

DOI 10.15252/embj.2020106777 | Received 12 September 2020 | Revised 31 March 2021 | Accepted 1 April 2021 | Published online 17 May 2021

The EMBO Journal (2021) 40: e106777

Introduction

The INK4a/ARF (CDKN2A) gene locus on human chromosome 9p21 encodes two structurally unrelated proteins with distinct tumor suppressor functions, p14^{ARF} and p16^{INK4a}. While p16^{INK4a} blocks the kinase activity of CDK4/CDK6, thus preventing Rb phosphorylation and subsequently S-phase entry, p14^{ARF} exerts p53-dependent and p53-independent cell cycle arrest and apoptosis (Kim & Sharpless, 2006). Consistent with these functions, the *INK4a/ARF* locus is frequently mutated in human malignancies, e.g., in ≥ 80% of sporadic pancreatic ductal adenocarcinomas (PDACs; Hezel *et al*, 2006), indicating that inactivation of this locus is essential for abnormal cell proliferation and loss of genomic stability.

p14^{ARF} is an important sensor of different types of cellular stress and hence positively regulated in response to oncogenic signals and genotoxic stress (Ozenne *et al*, 2010). In unstressed healthy cells, p14^{ARF} is usually expressed at low levels as a result of efficient N-terminal ubiquitination and subsequent proteasomal degradation (Kuo *et al*, 2004; Chen *et al*, 2010). Moreover, in the absence of DNA damage, p14^{ARF} is sequestered in the nucleoli due to its interaction with the abundant nucleolar protein NPM (nucleophosmin) leading to a functionally inactive, but more stable protein fraction (Rodway *et al*, 2004; Korgaonkar *et al*, 2005). Upon genotoxic stress, p14^{ARF} redistributes from the nucleolus to the nucleolar and cytoplasm, where it, among others, promotes activation of the p53 pathway by inhibiting the E3 ubiquitin ligase MDM2 (Lee *et al*, 2005; Sherr, 2006). Importantly, p14^{ARF} governs also tumor-suppressive activities independent of p53 and interacts with a variety of proteins, such as TIP60, TOPO I, and p32 (C1QBP), thereby regulating their function in DNA damage signaling, DNA repair, and

1 Institute for Molecular Biology and Tumor Research (IMT), Philipps-University Marburg, Marburg, Germany

2 Department of Visceral, Thoracic and Vascular Surgery, University Hospital Marburg, Philipps-University Marburg, Marburg, Germany

3 Core Facility Flow Cytometry, University Hospital Marburg, Philipps-University Marburg, Marburg, Germany

4 Institute for Med. Microbiology & Hospital Hygiene, University Hospital Marburg, Philipps-University Marburg, Marburg, Germany

5 Leibniz Institute of Molecular Pharmacology, Berlin, Germany

6 Institute of Molecular Immunology, Helmholtz Zentrum München, German Research Center for Environmental Health, München, Germany

7 Monoclonal Antibody Core Facility, Institute for Diabetes and Obesity, Helmholtz Zentrum München, German Research Center for Environmental Health, Neuherberg, Germany

8 Institute for Pathology, University Hospital Marburg, Philipps-University Marburg, Marburg, Germany

*Corresponding author. Tel: +49 6421 2865325; Fax: +49 6421 2865196; E-mail: bauer@imt.uni-marburg.de

[†]These authors contributed equally to this work.

apoptosis (Karayan *et al*, 2001; Ayrault *et al*, 2003; Eymin *et al*, 2006; Itahana & Zhang, 2008). Enforced nucleolar retention of p14^{ARF} inhibits these tumor-suppressive activities (Korgaonkar *et al*, 2005). The molecular mechanisms, which lead to the stress-induced redistribution of p14^{ARF}, have not been elucidated.

Targeting of p14^{ARF} to the nucleus and nucleolus is mediated by an arginine-rich sequence motif (amino acids 85–101) in its C-terminus (Zhang & Xiong, 1999; Rizos *et al*, 2000). Tumor-associated mutations of several arginine residues within this nuclear/nucleolar localization sequence (NLS/NoLS) have been reported to cause an altered subcellular localization of the protein. These NLS/NoLS mutations disrupt the p53-independent pro-apoptotic functions of p14^{ARF}, for example, attenuating p32-mediated apoptosis (Itahana & Zhang, 2008). The fact that p14^{ARF} is a highly basic protein, overall composed of 20% arginine residues, raises the question whether arginine methylation participates in the functional regulation of p14^{ARF}. The enzymes responsible for this post-translational modification are the protein arginine methyltransferases (PRMTs), which constitute a family of nine members in mammals (Yang & Bedford, 2013). They transfer methyl groups from the ubiquitous methyl-group donor S-adenosyl-L-methionine (SAM) to the terminal guanidino nitrogens of arginine residues, catalyzing monomethyl arginine (MMA), asymmetric dimethyl-arginine (ADMA), or symmetric dimethyl-arginine (SDMA). A multitude of nuclear and cytoplasmic proteins are post-translationally modified by arginine methylation. Thereby, PRMTs regulate a wide range of essential cellular processes, for example, signal transduction, nucleo-cytoplasmic transport, transcriptional regulation, and RNA splicing (Yang & Bedford, 2013).

In the present study, we investigated the potential impact of arginine methylation on the function of p14^{ARF}. We show that p14^{ARF} is arginine-methylated *in vivo* and that PRMT1 is responsible for the generation of ADMA-modified p14^{ARF}. Using mass spectrometry, we identified four arginine residues (R87/88/96/99) within the NLS/NoLS of p14^{ARF} as the major methylation sites of PRMT1. Overexpression or depletion of PRMT1 leads to perturbed subcellular localization and turnover of endogenous p14^{ARF} and defects in apoptosis signaling. Moreover, mutation of these PRMT1 methylation sites to amino acids that do not preserve the basic charge causes relocalization of the mutant p14^{ARF} proteins from the nucleoli to the nucleolar and cytoplasm. Genotoxic stress, such as UVC irradiation, results in an enhanced interaction between PRMT1 and p14^{ARF} and concomitantly increased levels of arginine-methylated p14^{ARF}, which contribute to the release from its nucleolar binding partner NPM. In addition, arginine methylation of p14^{ARF} enforces its interaction with the pro-apoptotic factor p32 and promotes apoptosis. Our data suggest that PRMT1-mediated arginine methylation causes crucial changes in the interaction network of p14^{ARF} and triggers stress-induced relocalization and tumor-suppressive functions of p14^{ARF}. Finally, we find that the PRMT1-p14^{ARF} cooperation is cancer-relevant and indicative for PDAC prognosis and chemotherapy response of pancreatic tumor cells.

Results

Arginine residues in p14^{ARF} are methylated by PRMT1 and PRMT5

Given that cancer-associated mutations of certain arginine residues within p14^{ARF} disclose an important role in the regulation of

apoptosis (Itahana & Zhang, 2008), we raised the question whether p14^{ARF} is arginine methylated and whether this post-translational modification is relevant for its tumor suppressor function. To this end, we analyzed the occurrence of *in vivo* methylation of p14^{ARF} by metabolic labeling. EGFP-tagged p14^{ARF} and empty vector (control) expressing HEK293 cells (Appendix Fig S1A) were cultured in the presence of L-[³H-methyl]-methionine, which is intracellularly metabolized to SAM. Additionally, cells were treated with translational inhibitors to avoid incorporation of radiolabelled methionine by *de novo*-protein biosynthesis (Liu & Dreyfuss, 1995). Subsequent to immunoprecipitation and SDS-PAGE, p14^{ARF} methylation was detected by fluorography, as depicted in Fig 1A (upper panel). Treatment with the global methyltransferase inhibitor adenosine dialdehyde (AdOx) resulted in hypomethylated cell extracts and in the loss of detection of methylated p14^{ARF} (Appendix Fig S1B, Fig 1A, upper panel). The overexpression and precipitation of EGFP-tagged p14^{ARF}, which typically occurred in a doublet band, were verified by Western blot analysis (Fig 1A, lower panel). Since p14^{ARF} does not contain any lysine residues, but a high number of arginines, this result indicates that p14^{ARF} is methylated at arginine residues *in vivo*.

To identify responsible PRMTs, we performed *in vitro* methyltransferase (MT) assays using bacterially expressed and purified GST-tagged p14^{ARF} and PRMTs (expressed/purified either from E.coli, mammalian cells or Sf9 cells) in the presence of radiolabeled methyl-group donor SAM. Here, PRMT1 and PRMT5 were found to methylate p14^{ARF}, whereas PRMT4 did not modify the protein (Fig 1B and C). PRMT1 and PRMT5 are known to share common substrates, but deposit different dimethylation marks, ADMA, and SDMA, respectively, which elicit diverse functional properties (Favia *et al*, 2019). In the present study, we focussed on the role of PRMT1-mediated methylation of p14^{ARF}. Using recombinant GST-tagged p14^{ARF} deletion constructs, we mapped the methylation sites of PRMT1 within the C-terminus of p14^{ARF} (aa 65–132), which encompasses an arginine-rich NoLS/NLS, whereas the N-terminal region (aa 1–64) also containing a basic charged NoLS/NLS was not modified by PRMT1 (Fig 1D). Mass-spectrometric analysis of *in vitro* methylated full-length GST-tagged p14^{ARF} protein was performed to identify the specific arginine residues that are modified by PRMT1. After tryptic digestion, LC-MS/MS identified two arginine residues (R96/R99) within the NoLS/NLS of p14^{ARF} as the major mono- and dimethylation sites (Fig 1E). In addition, fragment ion spectra provided some evidence of methylation of arginine 87 and 88 (R87/R88) with a lower degree of modification (data not shown). Remarkably, these four amino acid positions overlap with published cancer-associated mutations within the C-terminus of p14^{ARF} (Zhang & Xiong, 1999). Mutation of the four arginines to glycines in the full-length p14^{ARF} protein (p14^{ARF} RG) abolished *in vitro* methylation by PRMT1 and confirmed that PRMT1 predominantly modifies these four arginines in p14^{ARF} (Fig 1F). Furthermore, co-immunoprecipitation experiments showed that overexpressed Myc-tagged PRMT1 and Flag-tagged p14^{ARF} interact in U2OS cell extracts (Fig 1G). These results identify p14^{ARF} as a novel substrate and interaction partner of PRMT1.

PRMT1 regulates the cellular localization of p14^{ARF}

Given that p14^{ARF} is arginine methylated within its C-terminal NLS/NoLS by PRMT1, we investigated the subcellular localization

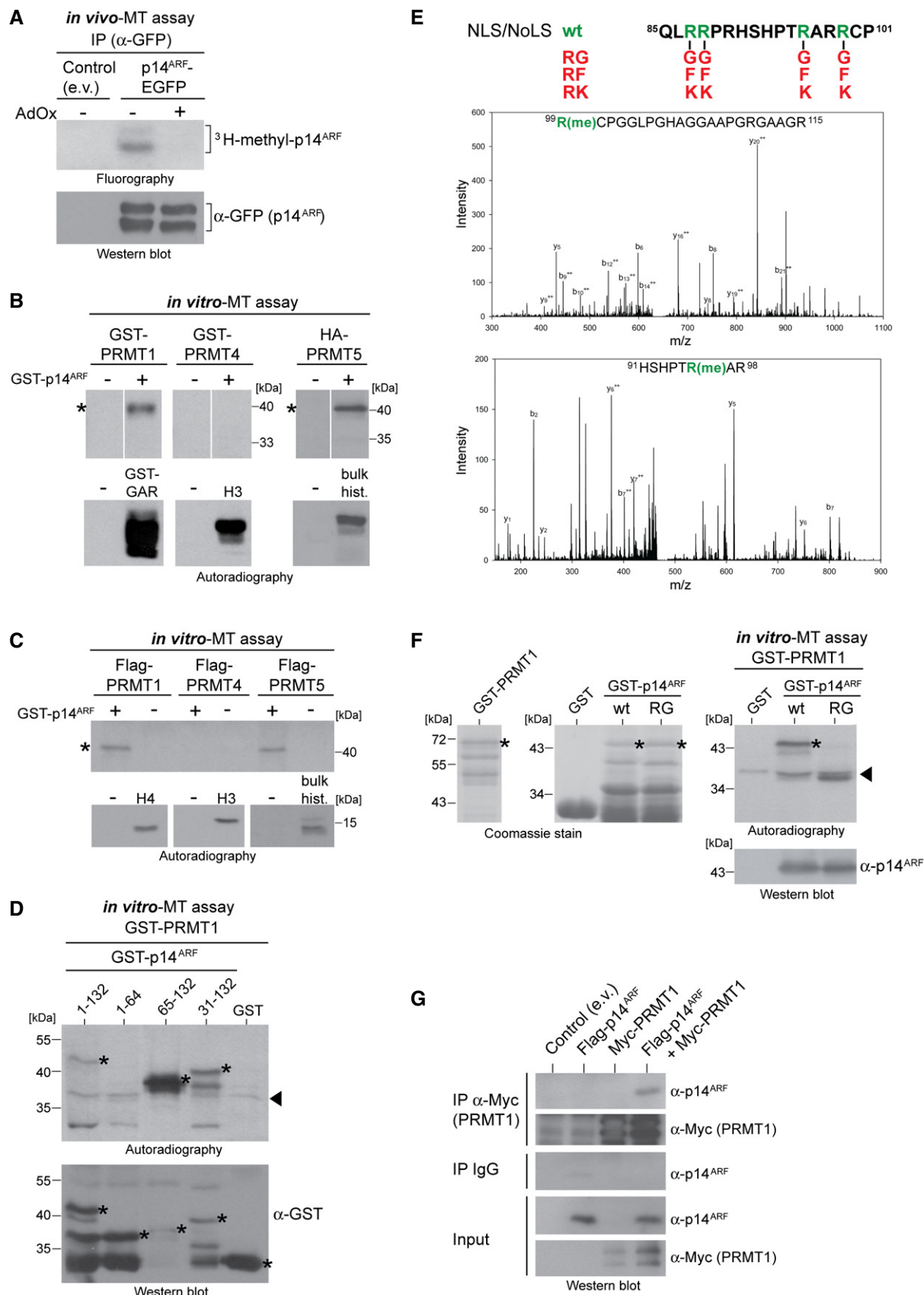


Figure 1.

Figure 1. Arginine methylation of p14^{ARF} by PRMT1.

- A For *in vivo* methyltransferase (MT) assay, HEK293 cells were transfected with either empty vector (e.v., control) or EGFP-tagged p14^{ARF}-containing plasmid. Subsequently, cells were treated with the global methyltransferase inhibitor adenosine dialdehyde, AdOx (+) or left untreated (-) for 72 h and then cultured in the presence of L-[³H-methyl]-methionine. Cell lysates were subjected to α -GFP immunoprecipitation (IP) and then assayed by fluorography (upper panel) and immunoblotting using α -GFP antibody (lower panel). EGFP-epitope tagged p14^{ARF} typically migrated as a doublet band, indicated by the bracket. Corresponding Appendix Fig S1 confirms p14^{ARF} overexpression in the cell lysates and hypomethylation caused by AdOx treatment.
- B Recombinant GST-tagged substrates (p14^{ARF}, GAR) and PRMT1/PRMT4 enzyme purified from bacteria or PRMT5 overexpressed/immunoprecipitated from HeLa cells (HA-tagged PRMT5/Myc-tagged MEP50) were subjected to *in vitro* methyltransferase (MT) assays in the presence of [¹⁴C-methyl]-SAM. Reactions were separated by SDS-PAGE, blotted, and assayed by autoradiography. GST-GAR, histone H3, and bulk histones served as a positive control for PRMT1, PRMT4, and PRMT5 activity, respectively. The two depicted negative controls (-) for PRMT1 are identical. The asterisks indicate the methylated p14^{ARF} protein. Corresponding autoradiography results show representative images and derive from the same blots and exposure times with white lines indicating where tracks were cut. Size markers (in kDa) are shown on the right.
- C Recombinant GST-tagged p14^{ARF} purified from bacteria and Flag-tagged PRMT1, PRMT4, or PRMT5 enzyme purified from baculoviral infected Sf9 cells were subjected to *in vitro* methyltransferase (MT) assays in the presence of [¹⁴C-methyl]-SAM. Reactions were separated by SDS-PAGE, blotted and assayed by autoradiography. Histone proteins H4, H3 and bulk histones served as a positive control for PRMT1, PRMT4 and PRMT5 activity, respectively. The asterisk indicates the methylated p14^{ARF} protein. Size markers (in kDa) are shown on the right.
- D GST-tagged full-length ORF (aa 1–132) and deletion constructs (aa 1–64, aa 65–132, and aa 31–132) of p14^{ARF} as well as GST alone were subjected to *in vitro* MT assays in the presence of GST-PRMT1 as described in (B). Methylation activities were detected by autoradiography (upper panel). Asterisks indicate methylated p14^{ARF} proteins, whereas the arrowhead marks p14^{ARF}-unrelated background signals (likely deriving from PRMT1 automethylation). Amounts of p14^{ARF} proteins and GST alone were visualized by immunoblotting using α -GST antibody (lower panel). Asterisks highlight the expected size and location of the different proteins. Size markers (in kDa) are shown on the left.
- E NLS/NoLS of p14^{ARF} (aa 85–101) is depicted at the top, with the PRMT1-methylated arginine residues distinguished in green and mutations to glycine (G), phenylalanine (F), or lysine (K) in red. For mass spectrometry, GST-tagged p14^{ARF} (full-length protein) was *in vitro* methylated by PRMT1, separated by SDS-PAGE, in-gel digested with trypsin and analyzed by LC-MS/MS. Fragment ion spectrum resulted from the doubly charged precursor ion of the R99-methylated (upper panel) and the R96-methylated (lower panel) p14^{ARF} peptides showing y-ions and b-ions by consecutive fragmentation reactions. Relevant ions were labeled according to the accepted nomenclature. Dimethylation of R99 was confirmed by detection of methylated N-terminal b-ions and unmethylated C-terminal y-ions. Dimethylation of R96 was detected in the mass of the b7, y6 and y7 ions.
- F Full-length GST-tagged wild-type (wt) and RG mutant p14^{ARF} protein, GST alone as well as GST-PRMT1 were purified from bacteria, as visualized by SDS-PAGE and Coomassie Blue staining (left and middle panel), with asterisks indicating the corresponding PRMT1 and p14^{ARF} protein bands. GST and GST-p14^{ARF} proteins (wt, RG) were subjected to *in vitro* MT assays in the presence of GST-PRMT1 as described in (B). Methylation activities were detected subsequent to protein blotting by autoradiography (upper right panel). The asterisk highlights the methylated p14^{ARF} wt protein, whereas the arrowhead indicates p14^{ARF}-unrelated background signals (likely deriving from PRMT1 automethylation). Amounts of p14^{ARF} proteins were detected by immunostaining of the autoradiographed blot using α -p14^{ARF} antibody (lower right panel). Size markers (in kDa) are shown on the left.
- G U2OS cells were transfected with the indicated plasmids (e.v., empty vector/control). Immunoprecipitation (IP) from cell lysates was performed using α -Myc antibody (exogenous PRMT1) or IgG as negative control. IP reactions and input lysates were analyzed by immunoblotting using the indicated antibodies.

Source data are available online for this figure.

of endogenous p14^{ARF} in different human cells upon ectopic expression of PRMT1 by immunofluorescence staining. In control transfected HeLa cells, endogenous p14^{ARF} displayed predominantly nucleolar localization (*) with rare detection in the nucleolar and cytoplasm (<), as illustrated in Fig 2A. Upon overexpression of PRMT1, p14^{ARF} showed an altered cellular distribution, namely predominant localization in the nucleolar and cytoplasm (Fig 2A). This finding was further corroborated by cell counting, in which the cell number with exclusively nucleolar p14^{ARF} staining was strongly reduced upon PRMT1 overexpression (Fig 2B). The PRMT1-dependent alteration of p14^{ARF}'s localization was not due to nucleolar disruption, as staining of the nucleolar protein NPM indicates the regular presence of nucleoli also in PRMT1-overexpressing cells (Appendix Fig S2). Similar observations were obtained in U2OS cells, which do not endogenously express p14^{ARF} (Stott *et al*, 1998). Exogenous p14^{ARF} was primarily found in the nucleoli of U2OS cells (Fig 2C and D). Overexpression of PRMT1 coincided with a redistribution of p14^{ARF} to the nucleolar and cytoplasm, whereas this redistribution was diminished upon overexpression of catalytically inactive PRMT1 (Fig 2C–E). Moreover, siRNA-mediated depletion of PRMT1 resulted in a more pronounced, exclusively nucleolar localization of p14^{ARF} (Fig 2F–I). In the PRMT1 depletion analysis, p14^{ARF}'s relocation into the nucleoli was subtle due to the already predominant nucleolar localization of p14^{ARF} in the siControl transfected HeLa cells

(Fig 2H and I). Altogether, these results indicate that PRMT1 regulates the cellular localization of p14^{ARF} and that its methyltransferase activity contributes to this function.

The basic charge of the PRMT1-targeted arginine residues is important for the nucleolar localization of p14^{ARF}

To investigate whether the PRMT1-targeted arginine residues within the NLS/NoLS are important for mediating the cellular localization of p14^{ARF}, we established several methyl-deficient mutant p14^{ARF} proteins. To this end, the four arginines (R87/88/96/99) were either mutated to glycines (RG) or phenylalanines (RF), which do not preserve the basic charge, or to lysines (RK), which retain the basic charge, but cannot be methylated by PRMTs (Fig 1E). EGFP-tagged p14^{ARF} wild-type and mutant proteins were overexpressed in U2OS cells and their cellular distribution (either exclusively nucleolar, not-exclusively nucleolar but additionally nucleolar/cytoplasmic or exclusively cytoplasmic) was investigated. Mutation of the four arginines to lysines resulted in a mutant protein (p14^{ARF} RK) with predominant, exclusively nucleolar localization similar to the wild-type protein (Fig 3A and B). In contrast, p14^{ARF} RG- and RF-mutant proteins showed a significant redistribution from the nucleolar to the nucleolar and cytoplasm, with the p14^{ARF} RF mutant displaying the highest cell number with exclusive localization in the cytoplasm (Fig 3A and B). Our results conform with the literature (Rizos *et al*,

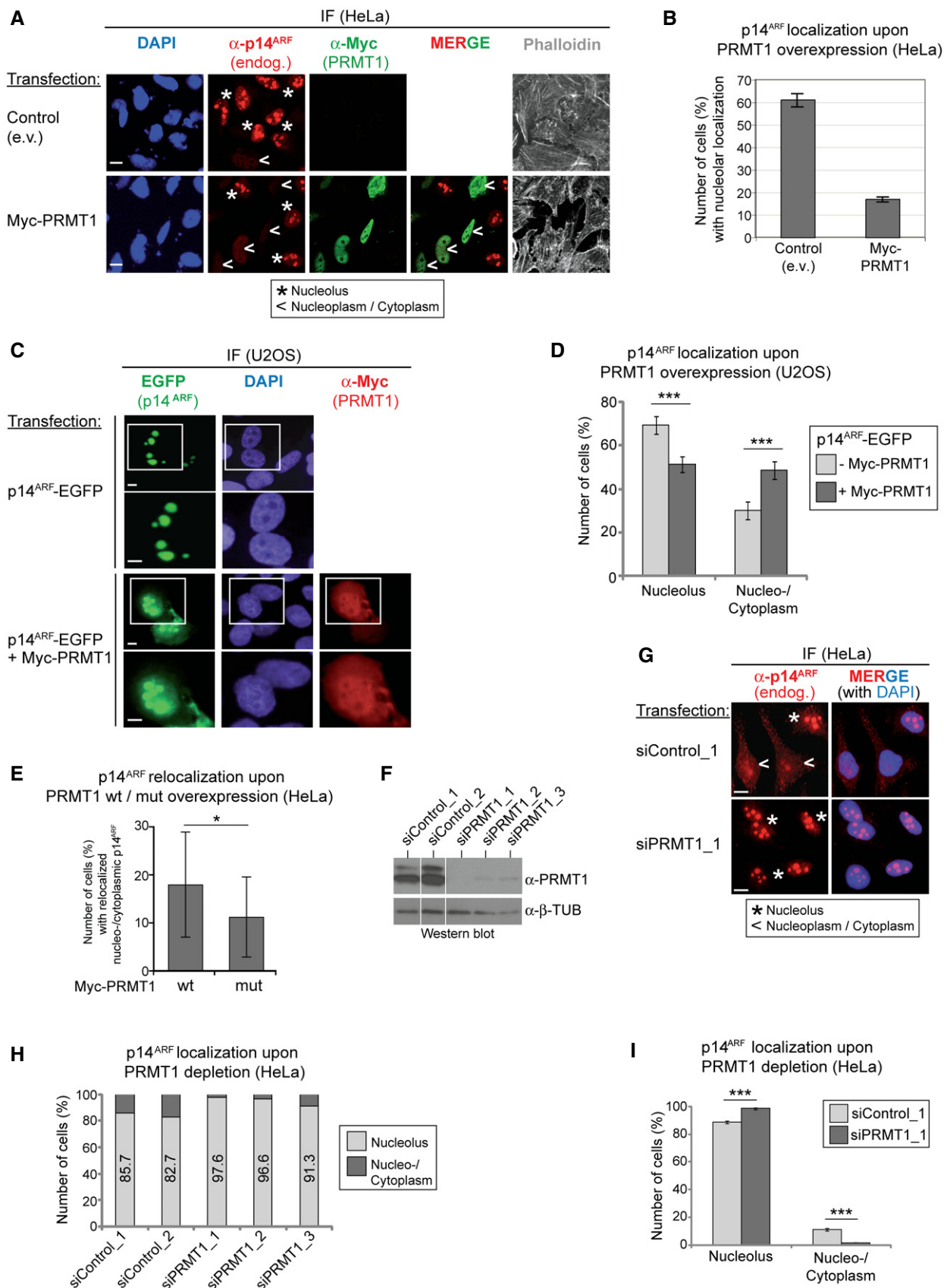


Figure 2.

Figure 2. PRMT1-dependent redistribution of nucleolar p14^{ARF}.

- A, B HeLa cells were transfected with empty vector (e.v., control) or Myc-tagged wild-type PRMT1-containing plasmid. Immunofluorescence (IF) staining was performed using α -p14^{ARF} (red, endogenous p14^{ARF}), α -Myc (green, exogenous PRMT1) antibodies, DAPI (blue, nuclei/DNA), and Phalloidin (gray, cytoplasm/F-actin). In (A), representative IF results are shown, with asterisks indicating cells with exclusive nucleolar and arrowheads indicating cells with predominantly nucleolar/cytoplasmic p14^{ARF} localization. The merge displays the combination of p14^{ARF} and PRMT1 staining. Scale bars: 15 μ m. The quantification of exclusive nucleolar p14^{ARF} was performed by cell counting (percentage of cells) and is shown for three independent experiments in (B) (mean \pm SD).
- C, D U2OS cells were transfected with EGFP-tagged p14^{ARF} alone or in combination with Myc-tagged wild-type PRMT1-containing plasmids. p14^{ARF}-EGFP (green), DAPI (blue, nuclei/DNA), and PRMT1 (red, using α -Myc antibody) were visualized by fluorescence microscopy, for which representative results are shown in (C), with the lower images displaying a magnification as indicated in the upper images by the rectangles. Scale bars: 10 μ m. The subcellular distribution of p14^{ARF}-EGFP (exclusively nucleolar or not-exclusively nucleolar but predominantly nucleolar/cytoplasmic) was quantified in p14^{ARF}-positive and p14^{ARF}/Myc-PRMT1-double-positive cells by cell counting (percentage of cells) for three independent experiments in (D) (mean \pm SD, *** P \leq 0.001 using Welch's t -test).
- E U2OS cells were transfected with EGFP-tagged p14^{ARF} alone or in combination with Myc-tagged wild-type (wt) or catalytically inactive (mut) PRMT1-containing plasmids. The cellular distribution of p14^{ARF}-EGFP was quantified as in (D). The relocalization of p14^{ARF} out of the nucleolus upon overexpression of PRMT1 (wt or mut) was determined by cell counting (percentage of cells) for four independent experiments (mean \pm SD, * P \leq 0.05 using the paired t -test).
- F–I HeLa cells were transfected with the indicated siRNAs (two control/non-targeting siRNAs and three PRMT1-specific siRNAs). PRMT1 depletion was verified by immunoblotting using α -PRMT1 and α - β -TUBULIN (loading control) antibodies (F); depicted staining results derive from the same blot as well as exposure times with white lines indicating where tracks were cut. The cellular p14^{ARF} distribution was determined by immunofluorescence staining (IF) using α -p14^{ARF} antibody. Representative IF images for the siControl_1 and siPRMT1_1 condition are shown in (G) (endogenous p14^{ARF} in red and the merge additionally with DAPI in blue for nuclei/DNA). Scale bars: 15 μ m. The subcellular localization of p14^{ARF} (exclusively nucleolar or not-exclusively nucleolar but predominantly nucleolar/cytoplasmic) was quantified by cell counting (percentage of cells) for all used siRNAs in (H) and for siControl_1/siPRMT1_1 from three independent experiments in (I) (mean \pm SD, *** P \leq 0.001 using Welch's t -test).

2000) that the basic charge of these arginine residues is crucial for the predominant nucleolar localization of p14^{ARF}.

To answer the question whether the four arginines R87/88/96/99 and their potential to be methylated are pivotal for the influence of PRMT1 on the p14^{ARF} localization, we determined the effect of PRMT1 overexpression on the relocalization of wild-type p14^{ARF} into the nucleolar and cytoplasm compared to p14^{ARF} RK. Thereby, exogenous PRMT1 caused a higher cell fraction with predominant nucleolar/cytoplasmic localization of wild-type p14^{ARF} compared to the RK mutant (Fig 3C). Thus, our results suggest that these specific arginines in the NLS/NoLS are important for the PRMT1-mediated redistribution of nucleolar p14^{ARF} into the nucleolar and cytoplasm, possibly due to their capability to be methylated.

Given that the nucleolar protein NPM has been reported to sequester p14^{ARF} in the nucleoli (Korgaonkar *et al*, 2005), we examined next whether the association of p14^{ARF} with NPM is influenced by PRMT1. Co-immunoprecipitation analyses showed that upon overexpression of PRMT1, endogenous p14^{ARF} interacts less efficiently with endogenous NPM in HeLa cell extracts, which was also confirmed in reciprocal precipitations (Fig 3D). Interestingly, NPM has previously been found to associate with multiple protein regions of p14^{ARF}, including also the C-terminus encompassing the arginine methylation sites of PRMT1 (Moulin *et al*, 2008). Therefore, we raised the question whether methylation of these arginines directly influences the interaction between p14^{ARF} and NPM. We performed peptide pull-down assays using two NLS/NoLS peptides of p14^{ARF} (aa 91–99 and aa 92–103) comprising the adjacent methylation sites R96 and R99, either unmodified or premodified by asymmetric dimethylation (single-modified R96me2a in peptide aa 91–99 and double-modified R96/R99me2a in peptide aa 92–103). Recombinant NPM protein displayed a binding preference for the unmodified NLS/NoLS peptides, whereas the single R96me2a and the double R96/R99me2a modification led to reduced NPM binding (Fig 3E). These data suggest that arginine methylation of the NLS/NoLS of p14^{ARF} by PRMT1 contributes to the release from its nucleolar binding partner NPM.

PRMT1 regulates p14^{ARF} protein stability

Previously, several reports showed that redistribution of nucleolar p14^{ARF} into the nucleolar and cytoplasm is accompanied by reduced protein stability (Rodway *et al*, 2004; Moulin *et al*, 2008). We therefore examined the protein levels of wild-type p14^{ARF} versus mutant proteins by Western blot. Of note, the α -p14^{ARF} antibodies used in this study were able to equally efficiently recognize p14^{ARF} wild-type and mutant (RG/RF/RK) proteins, as confirmed by Western blot analysis of recombinant GST-tagged p14^{ARF} proteins (Fig 1F, Appendix Fig S3A). Upon overexpression of the different p14^{ARF} proteins in various human cell lines, the p14^{ARF} RG and RF mutants showed strongly reduced protein levels compared to wild-type p14^{ARF} (Fig 4A), which was not due to diminished transcript levels of the RG and RF mutants (Fig 4B, Appendix Fig S3B and C). In contrast, the RK mutant displayed only moderately altered protein levels, which were not reflected by transcriptional changes in U2OS and HeLa cells, but in HEK293 cells. Furthermore, siRNA-mediated depletion of PRMT1 led to elevated endogenous p14^{ARF} protein levels, while overexpression of PRMT1 caused a reduction in p14^{ARF} protein levels (Fig 4C and D). Since these observations could also not be explained by an alteration of p14^{ARF} gene transcription (Appendix Fig S3D), we investigated whether PRMT1 influences p14^{ARF} protein stability. We applied doxycycline (Dox)-inducible shRNA to knock down endogenous PRMT1 in HeLa cells (Fig 4E) and monitored p14^{ARF} protein turnover following addition of the translational inhibitor cycloheximide (CHX). Depletion of PRMT1 upon doxycycline addition caused an increase in the level and stability of p14^{ARF} protein (Fig 4E–G). However, the interaction between p14^{ARF} and its reported ubiquitin ligases ULF, MKRN, and SIVA1 was not influenced by PRMT1 (data not shown; Chen *et al*, 2010; Ko *et al*, 2012; Wang *et al*, 2013). Together, these results indicate that PRMT1-mediated displacement of p14^{ARF} from the nucleolus leads to a reduction in protein stability likely due to its release from nucleolar sequestration (Rodway *et al*, 2004).

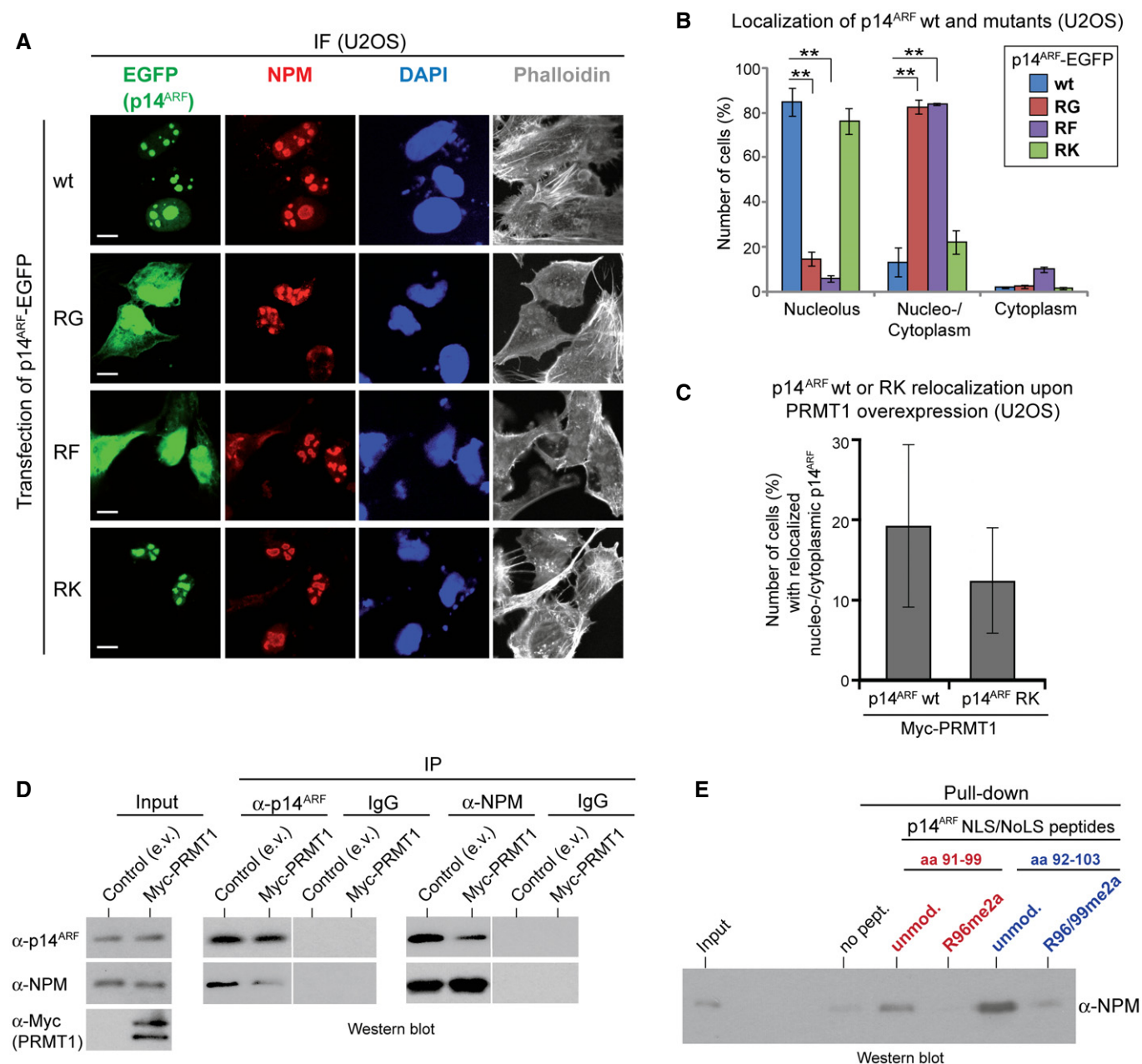


Figure 3. Involvement of the PRMT1-targeted arginines in p14^{ARF}'s nucleolar localization.

- A, B U2OS cells were transfected with EGFP-tagged wild-type (wt) or mutant (RG, RF, RK) p14^{ARF}-containing plasmids. p14^{ARF}-EGFP (green), endogenous NPM as a nucleolar marker (red, using α-NPM antibody), DAPI (blue, nuclei/DNA), and Phalloidin (gray, cytoplasm/F-actin) were visualized by fluorescence microscopy, for which representative results are shown in (A). Scale bars: 10 μm. The subcellular distribution of p14^{ARF}-EGFP (exclusively nucleolar, not-exclusively nucleolar but additionally nucleolus/cytoplasmic or exclusively cytoplasmic) was quantified by cell counting (percentage of cells) for three independent experiments in (B) (mean ± SD, ***P ≤ 0.005 using Welch's t-test).
- C U2OS cells were transfected with EGFP-tagged wild-type (wt) or mutant (RK) p14^{ARF}, either alone or in combination with Myc-tagged wild-type PRMT1-containing plasmids. Cells with predominant nucleolus/cytoplasmic localization of p14^{ARF}-EGFP (for both wt and RK) were quantified in the absence or presence of PRMT1 overexpression, i.e., in p14^{ARF}-positive as well as p14^{ARF}/Myc-PRMT1-double-positive cells, by immunofluorescence staining and cell counting. Relocalization of p14^{ARF} wt and RK into the nucleolus/cytoplasm upon overexpression of PRMT1 was defined in percentage of cells for five independent experiments (mean ± SD).
- D HeLa cells were transfected with empty vector (e.v., control) or Myc-tagged wild-type PRMT1-containing plasmid. Immunoprecipitation (IP) of endogenous p14^{ARF} or NPM was performed from cell lysates using the corresponding antibodies or IgG as negative control. IP reactions and input lysates were analyzed by immunoblotting using the indicated antibodies. Staining results of the IP reactions derive from the same blot and exposure times with the white lines indicating where tracks were cut.
- E Indicated NLS/NoLS p14^{ARF} peptides (aa 91–99 or aa 92–103) either unmodified or premodified (asymmetric dimethylation of R96 in peptide aa 91–99 and of R96/R99 in peptide aa 92–103) were covalently coupled to Sulfolink-beads and incubated with recombinant, baculoviral purified Flag-tagged NPM. Pull-down reactions and input of NPM protein were resolved by SDS-PAGE and analyzed by α-NPM immunoblotting.

DNA damage leads to PRMT1-dependent methylation of p14^{ARF}

Next, we investigated which cellular pathways might utilize the PRMT1-mediated regulation of p14^{ARF}'s function. Interestingly, when cells encounter genotoxic stress, p14^{ARF} has been described to

be activated, namely to redistribute from the nucleolar compartment to the nucleo- and cytoplasm, where it functions as a tumor suppressor, coinciding with decreased protein stability (Lee *et al*, 2005; Gallagher *et al*, 2006; Chen *et al*, 2013). To address whether stress-induced p14^{ARF} activation is influenced by PRMT1, we

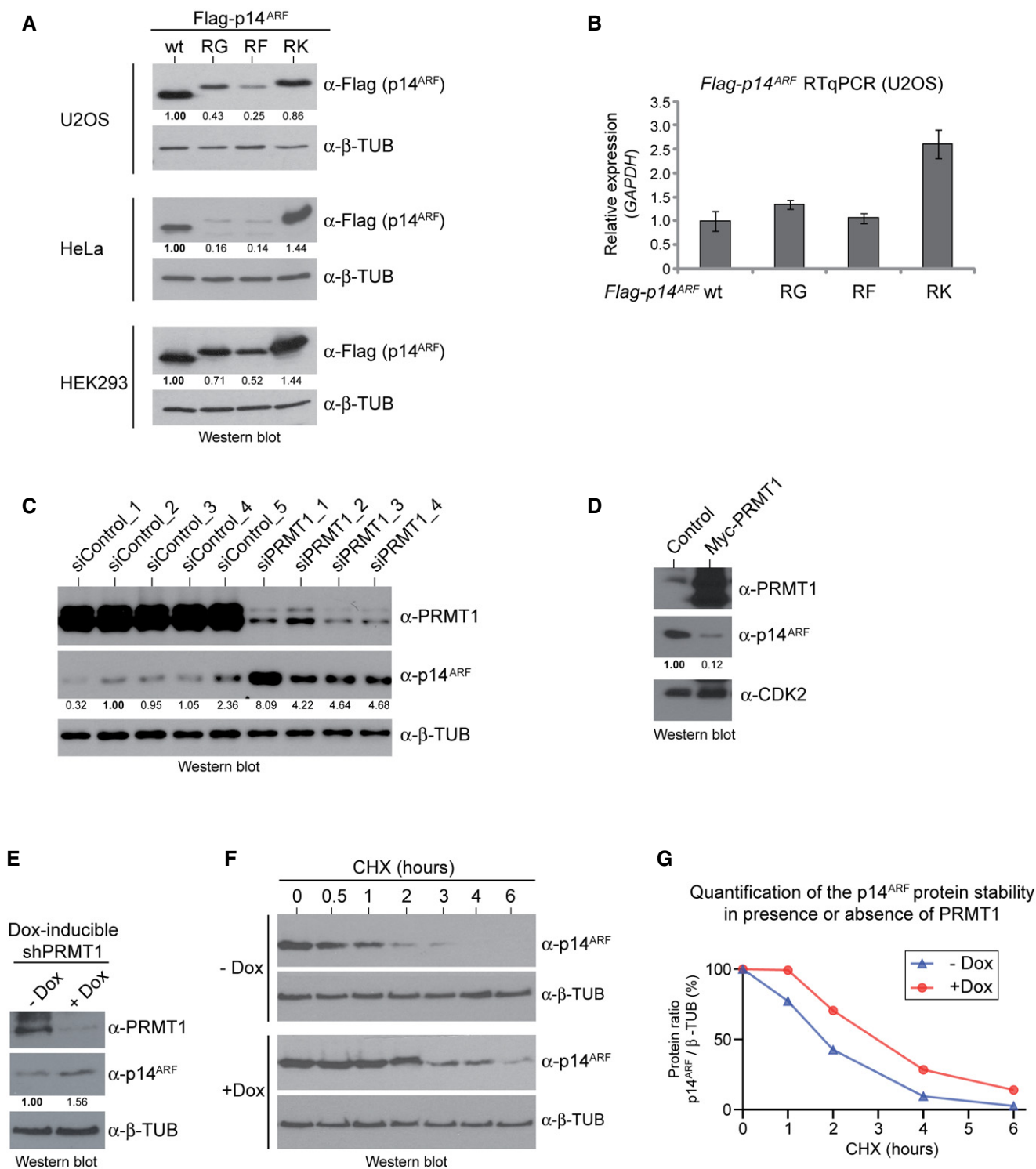


Figure 4.

Figure 4. Influence of PRMT1 and PRMT1-targeted arginines on p14^{ARF} protein stability.

- A, B U2OS, HeLa, and HEK293 cells were transfected with Flag-tagged wild-type (wt) or mutant (RG, RF, RK) p14^{ARF}-containing plasmids. Overexpression was analyzed by immunoblotting using α -Flag (exogenous p14^{ARF} proteins) and α - β -TUBULIN (loading control) antibodies (A). As visualized here, p14^{ARF} with the Flag-epitope tagged reproducibly showed a clear migration difference between wt and mutant p14^{ARF} proteins, with the mutants (especially the RK mutant) migrating slower than wt protein in the SDS-PAGE. The staining signals of the p14^{ARF} bands were densitometrically quantified and normalized to the respective β -TUBULIN signal, as specified by the numbers below the blots, with the protein signals of p14^{ARF} wt set to 1. Transcript levels of wt and mutant p14^{ARF} were determined by RT-qPCR in U2OS cells (B) as well as in HeLa and HEK293 cells (Appendix Fig S3B and C). Values were normalized to GAPDH expression and presented relative to wt p14^{ARF}, mean \pm SD of triplicates.
- C HeLa cells were transfected with the indicated siRNAs (five control/non-targeting siRNAs and four PRMT1-specific siRNAs). PRMT1 depletion and endogenous p14^{ARF} protein levels were analyzed by immunoblotting using α -PRMT1, α -p14^{ARF} and α - β -TUBULIN (loading control) antibodies. The p14^{ARF} signals were densitometrically quantified and normalized to the respective β -TUBULIN signal, as specified by the numbers below the blot, with the siControl_2 condition set to 1. Transcript levels of p14^{ARF} were determined by RT-qPCR (Appendix Fig S3D).
- D HeLa cells were infected with recombinant adenovirus encoding GFP (control) or wild-type PRMT1. PRMT1 overexpression and endogenous p14^{ARF} protein levels were analyzed by immunoblotting using α -PRMT1, α -p14^{ARF}, and α -CDK2 (loading control) antibodies. The p14^{ARF} signals were densitometrically quantified and normalized to the respective CDK2 signal, as specified by the numbers below the blot, with the control condition set to 1.
- E-G HeLa cells expressing a doxycycline-inducible shRNA targeting PRMT1 were treated or not with doxycycline (Dox) for 6 days. PRMT1 depletion was monitored by immunoblotting using the indicated antibodies (E). The p14^{ARF} signals were densitometrically quantified and normalized to the respective β -TUBULIN signal, as specified by the numbers below the blot, with the -Dox condition set to 1. PRMT1-proficient (-Dox) and PRMT1-depleted cells (+Dox) were further treated with the protein synthesis inhibitor cycloheximide (CHX) and harvested after 0, 0.5, 1, 2, 3, 4, and 6 h. Cell lysates were subjected to immunoblotting using α -p14^{ARF} and α - β -TUBULIN (loading control) antibodies and conventional ECL detection (F). For precise quantification of the p14^{ARF} protein stability in the -/+ Dox conditions during the CHX time course, immunoblotting was performed with independent cell lysates and primary antibodies, as in (F), which were then detected using fluorescence dye-coupled secondary antibodies and the LI-COR Odyssey system. The quantitative p14^{ARF} signals were normalized to the corresponding quantitative β -TUBULIN signals and displayed in (G). The CHX-untreated samples (0 h) were set to 100% for each condition.

irradiated wild-type and PRMT1-depleted HeLa cells with UVC and subsequently assessed p14^{ARF} localization by immunofluorescence staining. Upon exposure to UVC radiation, nucleolar staining of p14^{ARF} was strongly reduced in wild-type cells compared to the untreated condition (Fig 5A and B) in agreement with previous reports (Lee *et al*, 2005). However, PRMT1 depletion led to a higher accumulation of p14^{ARF} in the nucleolar compartment of unstressed cells, as observed before (Fig 2G-I). This effect was even more pronounced in UVC-stressed cells (Fig 5A and B) indicating that PRMT1 depletion antagonizes the UVC-induced redistribution of p14^{ARF} into the nucleolar and cytoplasm. Furthermore, PRMT1 knock-down increased the p14^{ARF} protein levels also in UVC-treated cells, which was not due to enhanced p14^{ARF} gene transcription (Fig 5C, Appendix Fig S4A). Similar results were obtained upon treatment with the DNA-damaging agent etoposide, where PRMT1 depletion counteracted the damage-stimulated relocalization and destabilization of p14^{ARF} (Appendix Fig S4B and C). Together, these data suggest that PRMT1-mediated p14^{ARF} regulation might be relevant for DNA damage-induced cellular responses.

To test this hypothesis, we screened commercially available pan-methyl-arginine antibodies, but could not identify any antibodies specifically binding methylated p14^{ARF}. We therefore generated a monoclonal methyl-arginine-specific antibody (α -me-p14^{ARF}) that recognizes the PRMT1-dependent methylation of R96 and R99 in p14^{ARF}, as validated by peptide dot blot analysis and Western blot analyses of *in vitro* MT assays, overexpressed wild-type p14^{ARF} versus RK mutant and PRMT1-depleted cell extracts (Appendix Fig S5A and Fig 5D and E, Appendix Fig S5B). By using the anti-me-p14^{ARF} antibody, we observed that UVC radiation caused an increase in the methylation of endogenous p14^{ARF} protein compared to low methylation levels in unstressed HeLa cells (Fig 5F). Detection of this DNA damage-induced methylation coincided with decreased p14^{ARF} protein levels indicating that p14^{ARF} methylation and p14^{ARF} protein stability counter-correlate. To address whether UVC-dependent arginine methylation of p14^{ARF} is mediated by

PRMT1, we established PRMT1 knockout and control HeLa cell lines using the CRISPR/Cas9 technology (Appendix Fig S6). Control cells displayed UVC-dependent methylation and reduced protein levels of endogenous p14^{ARF}, whereas PRMT1 knockout cells showed elevated p14^{ARF} protein levels and no detectable methylation of p14^{ARF} (Fig 5G). To ensure that this lower level of p14^{ARF} detected in control cells is actually caused by reduced protein levels and not by impaired antibody recognition of the endogenous protein due to epitope masking, we investigated the behavior of N-terminally Flag-tagged p14^{ARF} protein overexpressed in HeLa cells by α -Flag and α -p14^{ARF} immunostaining. The exogenous p14^{ARF} also exhibited an UVC-mediated reduction of its protein levels, similar to the endogenous p14^{ARF} protein (Appendix Fig S7). Consistent with the observation of a stress-dependent role of PRMT1 in p14^{ARF} regulation, the interaction between endogenous p14^{ARF} and endogenous PRMT1 was enhanced in co-immunoprecipitation experiments using wild-type HeLa cells upon UVC irradiation and coincided with endogenous p14^{ARF} methylation (Fig 5H). Altogether, these data suggest that genotoxic stress triggers the interaction between p14^{ARF} and PRMT1 accompanied by methylation and nucleolar release of p14^{ARF}, which results in a less stable but likely functionally active tumor suppressor protein.

Depletion of PRMT1 results in defects of apoptosis signaling

To assess whether PRMT1 influences the tumor suppressor activities of p14^{ARF}, such as cell cycle arrest and apoptosis induction, we examined the cell cycle distribution by flow cytometry using propidium iodide staining (PI-FACS) in PRMT1-depleted HeLa cells. In unstressed cells, siRNA-mediated depletion of PRMT1 did not cause significant changes in the cell cycle distribution compared to control cells (Fig 6A and B, Appendix Fig S8). Likewise, overexpression of wild-type p14^{ARF} and methyl-deficient mutant proteins (RG, RF, RK) caused a similar extent of G₁ phase arrest in U2OS cells (Appendix Fig S9A). Furthermore, wild-type p14^{ARF} and mutants

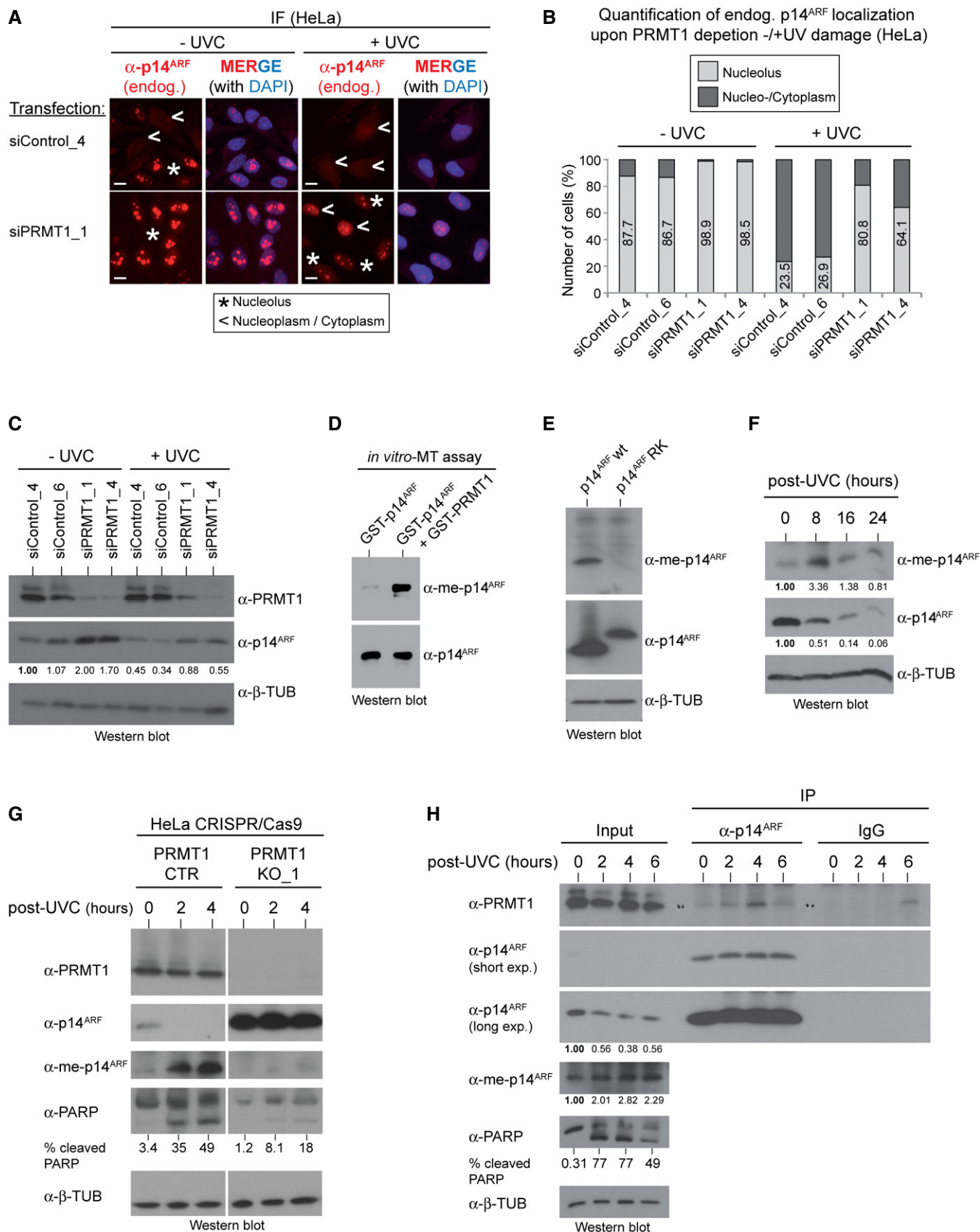


Figure 5.

Figure 5. PRMT1-dependent p14^{ARF} methylation in response to DNA damage.

- A–C HeLa cells were transfected with the indicated siRNAs (two control/non-targeting siRNAs and two PRMT1-specific siRNAs) and irradiated at 150 J/cm² UVC or not irradiated. After 24 h, the cellular distribution of endogenous p14^{ARF} was determined by immunofluorescence (IF) staining using α -p14^{ARF} antibody (red, endogenous p14^{ARF}) and in the merge additionally DAPI (blue, nuclei/DNA). Representative IF results are shown for two conditions (siControl_4 and siPRMT1_1) in (A), with asterisks indicating exclusively nucleolar and arrowheads indicating not-exclusively nucleolar but additionally or predominantly nucleolar/cytoplasmic p14^{ARF} localization. Scale bars: 15 μ m. The subcellular distribution of p14^{ARF}, as determined by IF, was quantified by cell counting (percentage of cells) for all conditions (B). PRMT1 depletion and p14^{ARF} protein levels were analyzed by immunoblotting using the indicated antibodies (C). The p14^{ARF} signals were densitometrically quantified and normalized to the respective β -TUBULIN signal, as specified by the numbers below the blot, with the siControl_4 condition set to 1.
- D GST-tagged p14^{ARF} and PRMT1 proteins purified from bacteria were subjected to an *in vitro* methyltransferase (MT) assay in the presence of SAM. Reactions were separated by SDS–PAGE and analyzed by immunoblotting using α -me-p14^{ARF} and α -p14^{ARF} antibodies.
- E U2OS cells were transfected with Flag-tagged wild-type (wt) or mutant (RK) p14^{ARF}-containing plasmids. Methylation and overexpression of p14^{ARF} were analyzed by immunoblotting using α -me-p14^{ARF}, α -p14^{ARF}, and α - β -TUBULIN (loading control) antibodies. The me-p14^{ARF} antibody predominantly recognizes the p14^{ARF} protein on the immunoblot, but weakly also other protein bands with higher molecular weights.
- F HeLa cells were irradiated at 150 J/cm² UVC. After 0, 8, 16, and 24 h, methylation of endogenous p14^{ARF} was analyzed by immunoblotting using α -me-p14^{ARF}, α -p14^{ARF}, and α - β -TUBULIN (loading control) antibodies. The methylated p14^{ARF} and the p14^{ARF} signals were densitometrically quantified and normalized to the respective β -TUBULIN signal, as specified by the numbers below the blots, with the not irradiated condition (0 h) set to 1.
- G HeLa cells either CRISPR/Cas9 control (CTR) or PRMT1-deleted (KO_1) were irradiated at 150 J/cm² UVC. After 0, 2, and 4 h, cell lysates were analyzed by immunoblotting using the indicated antibodies. Depicted staining results derive from the same blot and exposure times with white lines (between CTR and KO_1) indicating where tracks were cut. The percentage of PARP cleavage was densitometrically quantified and is indicated below the blot.
- H HeLa cells were irradiated at 150 J/cm² UVC. After 0, 2, 4, and 6 h, immunoprecipitation (IP) of endogenous p14^{ARF} was performed from cell lysates using α -p14^{ARF} antibody or IgG as negative control. IP reactions and input lysates were analyzed by immunoblotting using the indicated antibodies. Short and long exposure times are indicated. The p14^{ARF} and the methylated p14^{ARF} signals were densitometrically quantified and normalized to the respective β -TUBULIN signal, as specified by the numbers below the blots, with the not irradiated condition (0 h) set to 1. The percentage of PARP cleavage was also densitometrically quantified and is indicated below the blot.

equally stabilized p53 protein levels and showed the same capability to interact with the ubiquitin ligase MDM2 (Appendix Fig S9B–E). These results indicate that PRMT1-mediated arginine methylation of p14^{ARF} does not impact the cell cycle distribution of unstressed cells or the arrest functions of p14^{ARF} linked to p53 regulation.

Strikingly, upon UVC irradiation PRMT1-depleted HeLa cells displayed a significantly lower cell number in the subG₁ phase than control cells, as quantified by PI-FACS analysis (Fig 6A and B, Appendix Fig S8). Furthermore, in contrast to control cells, PRMT1-depleted cells showed no detectable increase of endogenous p14^{ARF} methylation upon UVC treatment (Fig 6C). To corroborate the observation on the pro-apoptotic effect of PRMT1 upon genotoxic stress, we investigated additional apoptosis markers in the PRMT1 knockout HeLa cell lines, i.e., PARP cleavage by Western blotting and Annexin V staining by flow cytometry. Consistently, the knockout cell clones showed diminished PARP cleavage and Annexin V-positive cell numbers upon UVC treatment compared to control clones (Fig 6D and E, Appendix Fig S10). To address whether PRMT1 promotes apoptosis via its methylation sites in p14^{ARF}, we overexpressed the nucleolar, basic charged p14^{ARF} RK mutant and the non-nucleolar p14^{ARF} RF mutant in PRMT1 knockout HeLa cells and exposed the cells to UVC irradiation. The apoptosis defect of PRMT1 knockout cells was more efficiently restored by the non-nucleolar RF mutant, which likely mimics functionally active p14^{ARF}, than by the nucleolar RK mutant (Fig 6F). These results suggest that PRMT1 and arginine methylation of p14^{ARF} contribute to the activation of apoptosis upon genotoxic stress.

Given that the PRMT1-mediated methylation of p14^{ARF} did not result in p53 activation, we hypothesized that the p53-independent tumor suppressor functions of p14^{ARF} are regulated by PRMT1. TIP60 and p32 have both been identified as direct interaction partners of p14^{ARF} that cooperate with p14^{ARF} to enable a p53-independent DNA damage response and apoptosis induction in cellular stress situations (Eymin *et al*, 2006; Itahana & Zhang, 2008). Using co-immunoprecipitation experiments, we found that the interaction between TIP60 and

p14^{ARF} is not influenced by PRMT1 or the RF mutation (Appendix Fig S11A and B). Remarkably, R87, R88, and R99 in p14^{ARF}, which we identified here as PRMT1 methylation sites, have been reported to mediate the interaction with the pro-apoptotic protein p32 (Itahana & Zhang, 2008). Cancer-derived mutations of these arginine residues disrupt the p14^{ARF}-p32 association and the pro-apoptotic function of p14^{ARF}. Using recombinant, purified proteins, we investigated in direct interaction assays whether the PRMT1-targeted arginines within p14^{ARF} influence its binding capability toward p32. The corresponding pull-down experiments revealed that the p14^{ARF} RF mutant, which *in vivo* seems to mimic functionally active p14^{ARF} (Fig 6F), exhibits a stronger interaction with p32 than wild-type p14^{ARF} (Fig 6G). Moreover, endogenous co-immunoprecipitation analyses showed that p14^{ARF} interacts less efficiently with p32 in PRMT1 knockout HeLa cell lines than in control cell lines (Fig 6H). These results suggest that PRMT1, likely via methylation of p14^{ARF}, enhances the interaction between p14^{ARF} and its pro-apoptotic binding partner p32 and thereby promotes p53-independent apoptosis.

PRMT1 expression levels are indicative for clinical PDAC prognosis and chemotherapy response of pancreatic tumor cells

Altered expression levels of PRMT1 have been reported in many human cancer types (Yoshimatsu *et al*, 2011). Given that our findings disclosed a novel tumor-suppressive activity of PRMT1, we investigated the clinical relevance of the PRMT1-p14^{ARF} connection in one of the most aggressive and lethal solid human tumors, namely PDAC. Initial survival analysis using the TCGA mRNA data set on PDAC (Anaya, 2016) indicated that high transcript levels of *PRMT1* correlate with an extended long-term survival of PDAC patients (> 500 days), whereas this correlation was not observed for the short-term survival group (< 500 days, Fig 7A). To enable comparative expression analyses of PRMT1 and p14^{ARF} on protein level in PDAC, we performed immunohistochemistry (IHC) stainings on surgical resection specimens of a cohort of 75 PDAC patients that

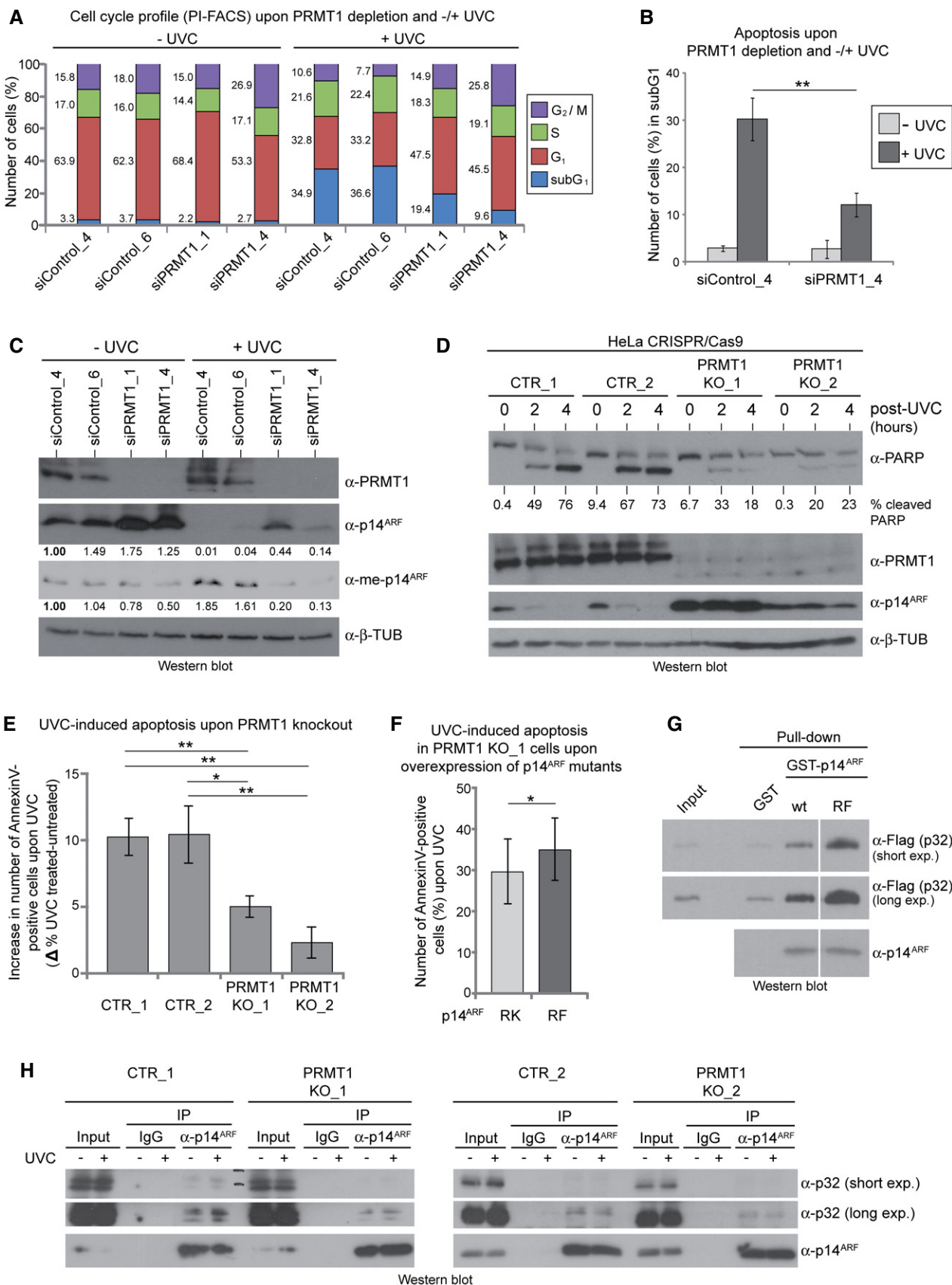


Figure 6.

Figure 6. Apoptosis regulation by PRMT1-mediated arginine methylation of p14^{ARF}.

- A–C HeLa cells were transfected with the indicated siRNAs (two control/non-targeting siRNAs and two PRMT1-specific siRNAs) and irradiated at 150 J/cm² UVC or not irradiated. After 24 h, cell cycle distribution was analyzed by flow cytometry using propidium iodide (PI) DNA staining for a representative experiment (A), Appendix Fig S8). The subG1 fraction of the siControl_4 and siPRMT1_4 condition was quantified for three independent experiments in (B) (mean ± SD, ***P* ≤ 0.005 using Welch's *t*-test). PRMT1 depletion and p14^{ARF} methylation of the samples (from (A)) were monitored by immunoblotting using the indicated antibodies (C). The p14^{ARF} and the methylated p14^{ARF} signals were densitometrically quantified and normalized to the respective β-TUBULIN signal, as specified by the numbers below the blots, with siControl_4 condition set to 1.
- D CRISPR/Cas9 control (CTR_1 and CTR_2) or PRMT1-deleted (KO_1 and KO_2) HeLa cell lines were irradiated at 150 J/cm² UVC. After 0, 2, and 4 h, cell lysates were analyzed by immunoblotting using the indicated antibodies. The percentage of PARP cleavage was densitometrically quantified and is specified below the blot.
- E CRISPR/Cas9 control (CTR_1 and CTR_2) or PRMT1-deleted (KO_1 and KO_2) HeLa cell lines were irradiated at 150 J/cm² UVC. After 4 h, the apoptotic cell fraction was analyzed by flow cytometry using FITC-labeled Annexin V and propidium iodide (PI). The increase in the apoptotic cell fraction upon UVC irradiation was quantified for three independent experiments (mean ± SD, ***P* ≤ 0.005 and **P* ≤ 0.05 using Welch's *t*-test).
- F HeLa CRISPR/Cas9 PRMT1 deleted (KO_1) cells were transfected with Flag-tagged-mutant RK or RF p14^{ARF}-containing plasmid and subsequently irradiated at 150 J/cm² UVC. After 4 h, the apoptotic cell fraction was quantified by flow cytometry using FITC-labeled Annexin V and propidium iodide (PI) for seven independent experiments (mean ± SD, **P* ≤ 0.05 using the paired *t*-test).
- G GST alone, GST-tagged wild-type (wt), and mutant (RF) p14^{ARF} proteins were coupled to Glutathione beads and incubated with baculoviral expressed, purified Flag-tagged p32. Pull-down reactions and input of p32 protein were resolved by SDS-PAGE and analyzed by immunoblotting using α-Flag and α-p14^{ARF} antibodies. Short and long exposure times are specified. Staining results derive from the same blot and exposure times with white lines indicating where tracks were cut.
- H CRISPR/Cas9 control (CTR_1 and CTR_2) or PRMT1-deleted (KO_1 and KO_2) HeLa cell lines were irradiated at 150 J/cm² UVC or not irradiated. After 4 h, immunoprecipitations (IP) of endogenous p14^{ARF} were performed from cell lysates using α-p14^{ARF} antibody or IgG as negative control. IP reactions and input lysates were analyzed by immunoblotting using the indicated antibodies. Short and long exposure times are specified.

all received post-operative adjuvant chemotherapy with gemcitabine. We scored the PRMT1 staining intensity in tumor cells of the PDAC tissues into three categories, namely highly elevated, moderately elevated and not elevated PRMT1 protein levels compared to the expression levels in normal pancreas tissue, which shows PRMT1 expression in pancreatic islet and acinar cells, but not in ductal cells (Fig 7B, Appendix Fig S12). In the present PDAC cohort, 45% of patients exhibited highly elevated, 32% moderately elevated, and 23% not elevated/normal PRMT1 protein levels (Fig 7C) indicating that the majority of PDAC patients (77%, *n* = 58) revealed elevated PRMT1 expression in their tumor cells. Moreover, elevated PRMT1 protein levels were positively correlated with survival. Of the 31 patients who survived at least 24 months after surgery, 55% displayed a highly elevated PRMT1 expression and 26% a moderately elevated PRMT1 expression, whereas only 19% showed a normal and not elevated PRMT1 expression (Fig 7D). On the opposite, 60% of patients with shorter survival times, for example, less than 12 months, exhibited not elevated or moderately elevated PRMT1 levels and only 40% showed highly elevated PRMT1 expression. These results suggest that very high PRMT1 expression levels correlate with a favorable prognosis of PDAC patients after potentially curative resection.

Given the here identified p14^{ARF}-mediated tumor-suppressive function of PRMT1, we hypothesized that PDAC patient survival might benefit from co-expression of p14^{ARF} with very high levels of PRMT1, but not with PRMT1 co-expressed at lower or not elevated levels in tumor cells. To this end, we determined the p14^{ARF} protein expression levels in the tumor cells of the PDAC cohort using immunofluorescence staining. We found that 29% of the patients exhibited a strong cytoplasmic/nuclear and pronounced nucleolar p14^{ARF} staining in their pancreatic neoplastic cells, indicating high p14^{ARF} expression levels similar to normal pancreas tissue (Fig 7E). Therefore, in this subgroup of PDAC patients, the tumor suppressor function of p14^{ARF} is likely to be relevant for chemotherapy response. The remaining 71% of PDAC specimens were scored as p14^{ARF}-negative, consistent with the literature reporting that the *CDKN2A* locus is very often inactivated in PDAC (Hezel *et al*, 2006).

Subsequent comparative analysis of the p14^{ARF} and PRMT1 protein levels in the PDAC cohort revealed that the percentage of patients co-expressing p14^{ARF} and highly elevated PRMT1 levels was considerably larger in the long-term survival group (35%, ≥ 24 months) than in the short-term survival group (12.5%, ≤ 12 months) (Fig 7F). In contrast, the percentage of p14^{ARF}-positive patients co-expressing not elevated or only moderately elevated PRMT1 levels was rather equal in the short-term (21%) and long-term (25%) survival group. These correlation analyses confirm our hypothesis that the long-term survival of PDAC patients might benefit from co-expression of p14^{ARF} with high PRMT1 levels, but not with low PRMT1 levels.

Given that PDAC patients generally undergo post-operative adjuvant chemotherapy with nucleoside analogues (gemcitabine or 5-fluorouracil as part of folirinox) to eradicate remaining tumor cells, we questioned next whether DNA damage caused by gemcitabine also triggers p14^{ARF} activation. Therefore, we initially examined several human pancreatic tumor cell lines for their p14^{ARF} expression. In agreement with the literature and the observation of a high mutation and inactivation rate of p14^{ARF} in primary PDACs (Hezel *et al*, 2006; Deer *et al*, 2010), we found that the majority of the tested cell lines do not express p14^{ARF}, such as MiaPaCa-2, S2-007 and Panc1 cells, but PaTu8988t cells showed high expression levels of p14^{ARF}, which was also predominantly localized in the nucleoli (Fig 8A, Appendix Fig S13). All PDAC cell lines tested expressed high levels of PRMT1 (Fig 8A). Remarkably, treatment of PaTu8988t cells with gemcitabine caused a redistribution of p14^{ARF} from the nucleolar compartment into the nucleolar and cytoplasm (Appendix Fig S14). Furthermore, this resulted in decreased protein levels and in increased p14^{ARF} methylation (Fig 8B and C), suggesting that p14^{ARF} acts also as a stress sensor in response to this kind of chemotherapeutic drugs. Therefore, we hypothesized that PRMT1 influences the efficiency of anti-cancer drugs such as gemcitabine. To this end, we treated p14^{ARF}-proficient (PaTu8988t) and p14^{ARF}-deficient (MiaPaCa-2) pancreatic tumor cell lines with gemcitabine in the absence or presence of the type I PRMT inhibitor MS023, which has been demonstrated to efficiently inhibit PRMT1 (Eram *et al*, 2016). Using Annexin V/propidium iodide staining and flow

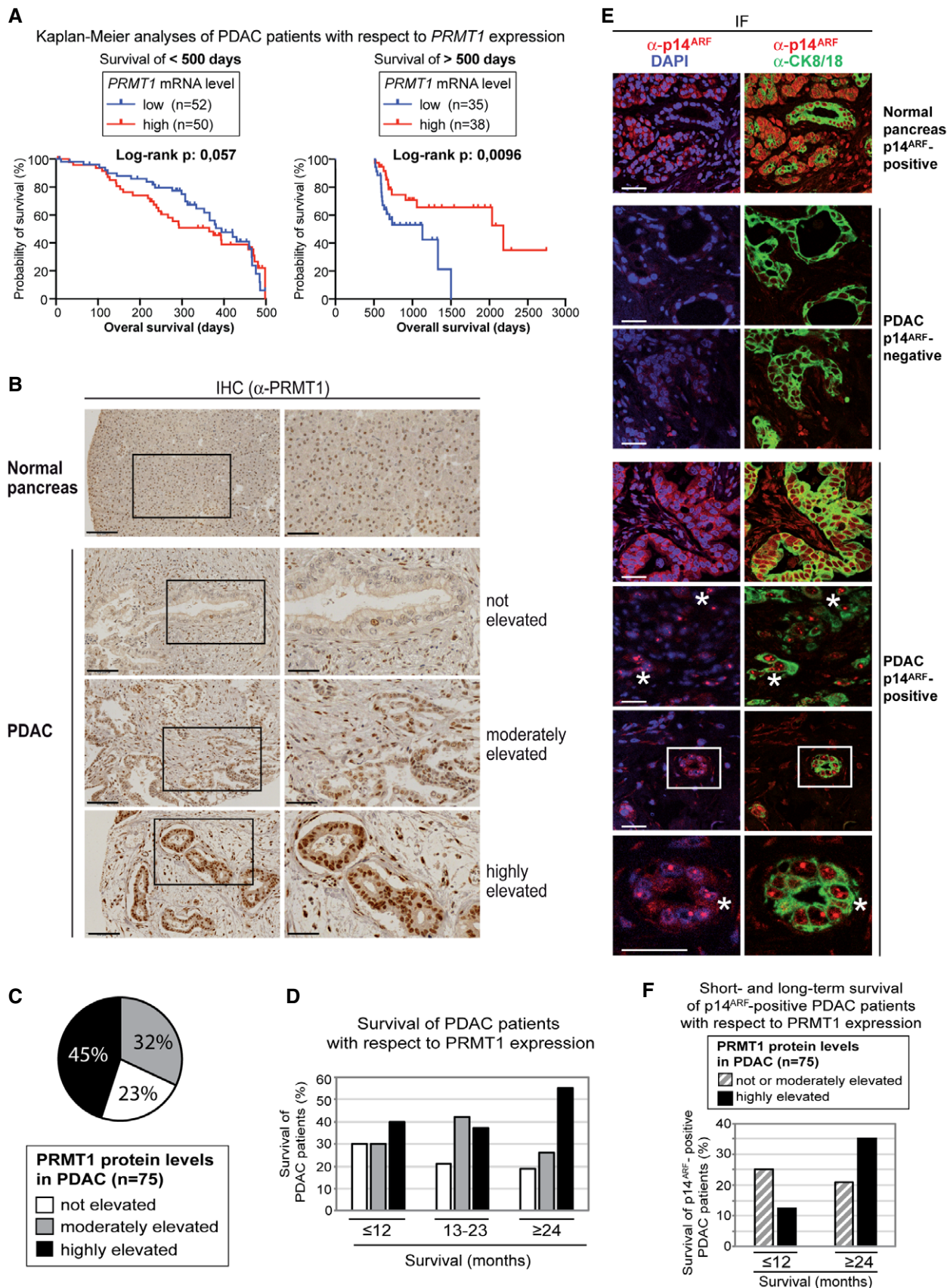


Figure 7.

Figure 7. Prognostic relevance of PRMT1 for clinical PDAC outcome.

- A Kaplan–Meier plot was generated using the transcriptome data set of PDAC from TCGA and OncoLnc to visualize the survival of PDAC patients with low or high *PRMT1* transcript levels and short-term (< 500 days, left plot) and long-term survival (> 500 days, right plot).
- B Representative immunohistochemistry (IHC) stainings of PRMT1 (brown) are shown for normal human pancreatic tissue and three PDAC specimens deriving from the cohort of 75 patients. Based on the immunostaining intensity and the percentage of stained tumor cells, all specimens were divided into three PRMT1 expression scores: not elevated, moderately elevated, and highly elevated PRMT1 expression in tumor cells in comparison with normal pancreas. Right images are magnifications of the left images, as indicated by the black rectangles. Scale bars in the left images: 100 μm . Scale bars in the right images: 50 μm .
- C The pie chart depicts the percentage of patients of the PDAC cohort ($n = 75$) belonging to the three PRMT1 expression scores: not elevated, moderately elevated, and highly elevated PRMT1 expression.
- D Patients of the PDAC cohort were grouped according to their survival time in months into three survival groups: short-term (≤ 12 months), medium-term (13–23 months), and long-term survivors (≥ 24 months). Subsequently, the percentage of patients belonging to the three different PRMT1 expression scores (legend as in (C)) are displayed for each survival group.
- E Immunofluorescence (IF) stainings of the 75 PDAC specimens were performed using α -p14^{ARF} (red), α -CK8/18 (green, staining ductal cells in normal pancreas and neoplastic cells in PDAC) antibodies and DAPI (blue, nuclei/DNA). Representative IF images are shown for normal human pancreatic tissue, two PDAC specimens displaying no p14^{ARF} expression and three PDAC specimens displaying strong p14^{ARF} expression in tumor cells. Left and corresponding right images show the same tissue section. Asterisks indicate nucleolar p14^{ARF} localization in neoplastic cells of PDAC. The last image pair shows a magnification of the image pair above (indicated by the rectangle). Scale bars: 35 μm .
- F p14^{ARF}-positive patients of the PDAC cohort were grouped according to their survival time in month into two survival groups: short-term (≤ 12 months) and long-term survivors (≥ 24 months). Subsequently, the percentages of patients with either not/moderately elevated PRMT1 expression or highly elevated PRMT1 expression are displayed for the two survival groups.

cytometry, we found that both p14^{ARF}-proficient and p14^{ARF}-deficient PDAC cells undergo cell death upon gemcitabine treatment (Fig 8D, Appendix Fig S15). However, co-treatment with MS023 resulted in diminished gemcitabine-induced cell death of PaTu8988t (p14^{ARF}-proficient), but not of MiaPaCa-2 cells (p14^{ARF}-deficient). Furthermore, addition of MS023 alone reduced the numbers of dead PaTu8988t cells compared to the untreated condition, which was not the case for MiaPaCa-2 cells. These observations in PaTu8988t cells were also corroborated by Western blot analysis of PARP cleavage, which was decreased upon co-treatment with gemcitabine and MS023 in comparison with single treatment with gemcitabine (Fig 8E). Moreover, MS023 treatment resulted in elevated p14^{ARF} protein levels, reminiscent of the effect caused by PRMT1 depletion or deletion (Figs 5C and G, and 6C and D).

Given that PaTu8988t and MiaPaCa-2 cells have accumulated multiple mutations, which might contribute to their specific apoptotic behavior apart from their PRMT1 and p14^{ARF} status, we generated PaTu8988t cells depleted for p14^{ARF} (Fig 8F) and MiaPaCa-2 cells exogenously expressing p14^{ARF} (Fig 8H). Both sets of isogenic cell lines were then analyzed for their ability to undergo gemcitabine-dependent apoptosis and for their response toward MS023 treatment. Control siRNA transfected PaTu8988t cells showed similarly to wild-type PaTu8988t cells (Fig 8D) that gemcitabine-induced apoptosis was diminished upon MS023 treatment (Fig 8G). In contrast, siRNA-mediated depletion of p14^{ARF} led to unchanged or increased gemcitabine-induced apoptosis of PaTu8988t cells in the presence of MS023 (Fig 8G), reminiscent of the behavior of p14^{ARF}-deficient MiaPaCa-2 cells (Fig 8D) indicating that p14^{ARF} and PRMT1 cooperate in apoptosis induction of PaTu8988t cells. Overexpression of p14^{ARF} in MiaPaCa-2 cells did not change the apoptotic rate in the untreated condition (Fig Appendix S16), but strikingly, resulted in reduced levels of MS023- and MS023/gemcitabine-mediated apoptosis compared to control transfected cells (Fig 8I), thereby converting the apoptotic behavior of these cells into that of p14^{ARF}-proficient PDAC tumor cells. PRMT1 activity seems to contribute to an efficient chemotherapy response, at least in the context of certain cancer cell genome states, e.g., in the presence of wild-type p14^{ARF}. Altogether, our results reveal that p14^{ARF} and PRMT1 functionally cooperate in

their tumor-suppressive activities *in vivo* and that their synergy might be relevant for tumor prognosis and clinical outcome of PDAC.

Discussion

In the present study, we identify the tumor suppressor protein p14^{ARF} as a novel interaction partner and substrate of PRMT1. Our findings show that the interaction between PRMT1 and p14^{ARF} is reinforced upon genotoxic stress leading to arginine methylation of the NoLS/NLS in p14^{ARF} (Fig 9). This methylation event concomitantly causes crucial changes in the interaction network of p14^{ARF}. On the one hand, p14^{ARF} methylation weakens the association with its nucleolar interaction partner NPM and enables its release from the nucleolar compartment. Upon relocalization to the nucleolar and cytoplasm p14^{ARF} becomes functionally active, albeit less stable. On the other hand, the stress-induced methylation of p14^{ARF} seems to enforce its interaction with the pro-apoptotic factor p32 and promotes p53-independent apoptosis. Our data unravel PRMT1-mediated arginine methylation as an important trigger for the stress-induced tumor-suppressive function of p14^{ARF} (Fig 9).

Given that nothing is known so far about the mechanism leading to stress-induced arginine methylation of p14^{ARF}, we hypothesize that post-translational modifications, such as DNA damage-induced phosphorylation, might alter PRMT1's binding affinity and activity toward its substrate p14^{ARF}. Phosphorylation of PRMT1 has been reported to regulate protein–protein interactions and substrate specificity (Rust *et al*, 2014; Bao *et al*, 2017). Recently, replication stress stimulated by cisplatin treatment and other agents has been shown to induce a PRMT1-dependent arginine methylome in ovarian cancer cells (Musiani *et al*, 2020). Cisplatin exposure triggers the interaction between PRMT1 and DNA-PK, a kinase required for NHEJ (non-homologous end joining)-mediated DNA repair, leading to phosphorylation and concomitant chromatin recruitment of PRMT1. This stress-induced redirection of the activity of PRMT1 enhances methylation of histone H4 at arginine 3 (H4R3me) in chromatin and promotes the activation of a pro-inflammatory and cell cycle arrest gene expression program (Musiani *et al*, 2020).

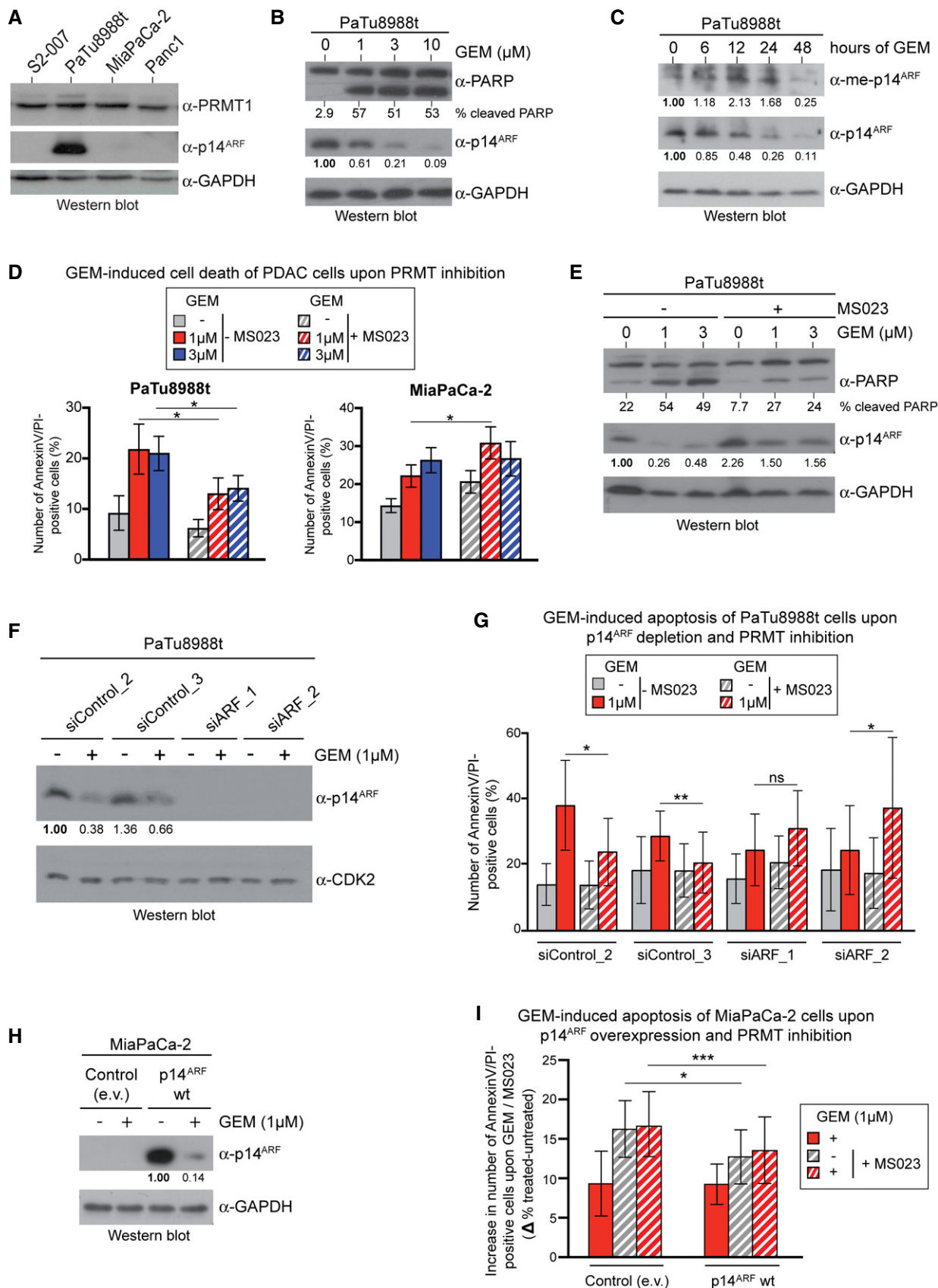
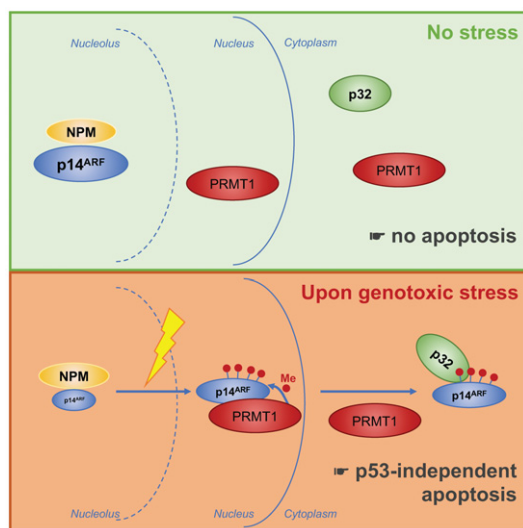


Figure 8.

Figure 8. Impact of PRMT1 on chemotherapy response and apoptosis induction of PDAC cell lines.

- A Cell lysates of the indicated human pancreatic tumor cell lines (S2-007, PaTu8988t, MiaPaCa-2, Panc1) were resolved by SDS-PAGE and analyzed by immunoblotting for p14^{ARF} (α -p14^{ARF}) and PRMT1 (α -PRMT1) protein levels. GAPDH staining served as loading control.
- B PaTu8988t cells were treated with 0, 1, 3, and 10 μ M gemcitabine (GEM). After 48 h, cell lysates were analyzed by immunoblotting using the indicated antibodies. The p14^{ARF} signals were densitometrically quantified and normalized to the respective GAPDH signal, as specified by the numbers below the blots, with the untreated condition (– GEM) set to 1. The percentage of PARP cleavage was also densitometrically quantified and is indicated below the blot.
- C PaTu8988t cells were treated with 3 μ M gemcitabine (GEM) or left untreated (0 h). After 0, 6, 12, 24, and 48 h, methylation of endogenous p14^{ARF} was analyzed by immunoblotting using α -me-p14^{ARF}, α -p14^{ARF}, and α -GAPDH (loading control) antibodies. The methylated p14^{ARF} and the p14^{ARF} signals were densitometrically quantified and normalized to the respective GAPDH signal, as specified by the numbers below the blots, with the untreated condition (0 h) set to 1.
- D, E PaTu8988t and MiaPaCa-2 cells were treated (+) with 20 μ M MSO23 or left untreated (–) for 3 days. For the last 2 days, the cells were additionally exposed to 0, 1, or 3 μ M gemcitabine (GEM). Subsequently, cell death was quantified by flow cytometry (in (D)) using FITC-labeled Annexin V and propidium iodide (PI) for four independent experiments (mean \pm SD, * P \leq 0.05 using Welch's t -test). Additionally, PaTu8988t cell lysates were analyzed by immunoblotting using the indicated antibodies. A representative result is displayed in (E). The p14^{ARF} signals were densitometrically quantified and normalized to the respective GAPDH signal, as specified by the numbers below the blots, with the untreated condition (– GEM, – MSO13) set to 1. The percentage of PARP cleavage was also densitometrically quantified and is indicated below the blot.
- F, G PaTu8988t were transfected with the indicated siRNAs (two control/non-targeting siRNAs and two p14^{ARF}-specific siRNAs) and treated (+) with 20 μ M MSO23 or left untreated (–) for 3 days. For the last 2 days, the cells were additionally exposed 1 μ M gemcitabine (+ GEM) or not (– GEM). p14^{ARF} depletion was monitored by immunoblotting using the indicated antibodies. A representative result is displayed in (F). The p14^{ARF} signals in the siControl conditions were densitometrically quantified and normalized to the respective CDK2 signal, as specified by the numbers below the blot, with the untreated condition (– GEM) of the siControl_2 sample set to 1. Apoptosis was quantified by flow cytometry (G) using FITC-labeled Annexin V and propidium iodide (PI) for six independent experiments (mean \pm SD, ** P \leq 0.005, * P \leq 0.05, ns: not significant using Welch's t -test).
- H, I MiaPaCa-2 cells were transfected with empty vector (e.v., control) or Flag-tagged wild-type (wt) p14^{ARF}-containing plasmid and treated (+) with 20 μ M MSO23 or left untreated (–) for 3 days. For the last 2 days, the cells were additionally exposed to 1 μ M gemcitabine (+ GEM) or not (– GEM). p14^{ARF} overexpression was monitored by immunoblotting using the indicated antibodies. A representative result is displayed in (H). The p14^{ARF} signals in the overexpression conditions were densitometrically quantified and normalized to the respective GAPDH signal, as specified by the numbers below the blot, with the untreated condition (– GEM) set to 1. Apoptosis was analyzed by flow cytometry (I) using FITC-labeled Annexin V and propidium iodide (PI). The increase in the apoptotic cell fraction upon gemcitabine and/or MSO23 was quantified for four independent experiments (mean \pm SD, *** P \leq 0.001, * P \leq 0.05 using Welch's t -test).

**Figure 9. Model for the regulation of the tumor suppressor protein p14^{ARF} by PRMT1.**

In unstressed cells, p14^{ARF} is predominantly sequestered in the nucleoli, bound to its nucleolar interaction partner NPM. Upon genotoxic stress, the interaction between p14^{ARF} and PRMT1 is reinforced and the C-terminal NLS/NoLS of p14^{ARF} is methylated by PRMT1. This stress-induced arginine methylation promotes the release of p14^{ARF} from NPM and nucleolar sequestration, leading to p53-independent apoptosis.

The relevance of the methylation sites in p14^{ARF} is emphasized by the fact that these arginine residues are frequently mutated in cancer, thereby disrupting the pro-apoptotic function of p14^{ARF} (Itahana & Zhang, 2008). Similarly, PRMT1 expression has been

reported to be altered, mostly upregulated, in many human tumors (Yoshimatsu *et al*, 2011; Yang & Bedford, 2013). PRMT1 is the most abundant PRMT member and responsible for generating the majority of arginine-methylated residues in mammalian cells (Tang *et al*, 2000). In agreement with its essential function in early embryonic development, PRMT1 regulates progenitor cell renewal and lineage commitment mainly on the level of transcriptional regulation by methylation of H4R3 and other chromatin proteins (Pawlak *et al*, 2000; Zhao *et al*, 2008; Bao *et al*, 2017; Blanc *et al*, 2017). On the one hand, in muscle stem cells, PRMT1 restricts the self-renewal capacity and promotes the myogenic differentiation program, whereas on the other hand the opposite is the case in epidermal stem cell, where PRMT1 is responsible for progenitor proliferation as well as maintenance and inhibits terminal differentiation (Bao *et al*, 2017; Blanc *et al*, 2017). Thus, depending on the cell lineage, PRMT1 executes opposing effects on proliferation and differentiation, either pro-proliferative and differentiation-blocking or anti-proliferative and differentiation-promoting activities. Consequently, in the context of carcinogenesis, it is conceivable that PRMT1 functions as an oncoprotein but also as a tumor suppressor protein. For example, in acute myeloid leukemia PRMT1 cooperates with cancer cell-specific transcription factors and coregulators, such as RUNX1 or oncogenic MLL-fusion proteins, leading to an aberrant pro-proliferative and tumor-promoting transcriptional response (Cheung *et al*, 2007, 2016; Shia *et al*, 2012).

Apart from affecting stem cell homeostasis and differentiation processes, PRMT1 is also involved in important cellular house-keeping functions, for example, in the maintenance of genome stability and DNA damage response, for example, by methylation of critical DNA repair proteins, such as MRE11, 53BP, and BRAC1 (Boisvert *et al*, 2005a, 2005b; Yu *et al*, 2009; Vadnais *et al*, 2018; Montenegro *et al*, 2020). In line with this protection function in

cellular stress situations, PRMT1 also regulates apoptosis by methylation of pro-apoptotic proteins, such as the transcription factor FOXO1 and the BCL-2 antagonist BAD. These methylation events inhibit AKT-dependent phosphorylation of FOXO1 and BAD, thereby enabling apoptosis induction (Yamagata *et al*, 2008; Sakamaki *et al*, 2011). Similarly, methylation of the transcription factor E2F-1 by PRMT1 stabilizes the protein during DNA damage and fosters E2F-1-dependent apoptosis (Zheng *et al*, 2013). Our findings on the pro-apoptotic cooperation between PRMT1 and p14^{ARF} integrate into the general perspective that the cellular activities of PRMT1 upon DNA damage are anti-proliferative and activate tumor suppressor functions.

In cancer cells, in which PRMT1 mainly acts as an oncoprotein by stimulating proliferation, blocking differentiation and apoptosis or enhancing DNA repair efficiency, pharmacological inhibition of PRMT1 will likely be therapeutically beneficial (Guccione & Richard, 2019). In these cases, PRMT1 inhibition in combination with classic chemotherapy can help to prevent the PRMT1-driven oncogenic transcriptional responses and cancer cells from evading apoptosis. However, in cancer cells, in which the dominating stress-induced function of PRMT1, e.g., during chemotherapy treatment, is pro-apoptotic by methylation of p14^{ARF}, FOXO1, BAD, or E2F-1, PRMT1 inhibition is counterproductive and harmful. In the majority of human PDAC patients, we found elevated PRMT1 protein levels in agreement with recent reports (Wang *et al*, 2016; Song *et al*, 2020). Remarkably, PRMT1 expression levels positively correlated with an extended long-term survival of PDAC patients suggesting that the tumor-suppressive effects of PRMT1 might prevail in this tumor entity. Furthermore, PDAC patients benefited in their long-term survival from co-expression of p14^{ARF} with high levels of PRMT1, but not with lower levels of PRMT1. In agreement, p14^{ARF}-positive pancreatic tumor cells with high PRMT1 levels revealed increased gemcitabine-induced apoptosis rates compared to cells co-treated with a PRMT inhibitor, suggesting that here PRMT1 might contribute to an efficient chemotherapy response. Upregulation of PRMT1 during tumor cell evolution might be conducive to increase the tumor mass and malignancy, but PRMT1 inhibitor treatment should not be taken per se as a promising therapeutic strategy. Instead, further in-depth understanding of the molecular pathology and the accompanying genetic alterations of specific tumor entities is strictly necessary to decide on the advantage or disadvantage of pharmacological PRMT1 inhibition.

Materials and Methods

Cell lines and reagents

U2OS, HeLa, HEK293T, PaTu8988t, MiaPaCa-2, S2-007, and Panc1 cells were maintained in DMEM supplemented with 10% fetal calf serum (FCS, Gibco/BRL), 1% penicillin/streptomycin at 37°C and 5% CO₂. Sf9 cells were cultured as described in (Berberich *et al*, 2017). Detailed information on cell culture reagents, manipulations, plasmids, and antibodies (including the generation of α -me-p14^{ARF}) is supplied in the Appendix Supplementary Methods. Of note, all α -p14^{ARF} antibodies used in the present study were able to equally efficiently recognize unmethylated and methylated p14^{ARF} wild-type (Fig 5C) and the p14^{ARF}-mutant (RG/RF/RK) proteins (shown for α -

p14^{ARF} from Bethyl in Fig 1F, Appendix Fig S3A; data not shown for α -p14^{ARF} from Novus and Sigma).

Human tissue

Patient material was obtained from the Department of Surgery at the University Hospital Marburg and pancreatic tissue blocks were archived in the Department of Pathology. All patients provided written informed consent, and the study was approved by the Ethics Committee of the Philipps-University Marburg (No. 05/2003).

In vivo MT assay

For detection of *in vivo* methylation of p14^{ARF}, metabolic labeling of HEK293 cells was conducted in the presence of radiolabeled methionine, of which the ³H-labeled methyl-group is intracellularly metabolized and incorporated into the cofactor SAM, as described in (Liu & Dreyfuss, 1995). In detail, transfected HEK293 cells were initially cultured for 3 days in the absence or presence of AdOx (20 μ M). For translational block, cells were pretreated with 40 μ g/ml chloramphenicol (Sigma-Aldrich) and 100 μ g cycloheximide (AppliChem). After 30 min of pretreatment, L-[³H-methyl]-methionine (³H-methionine 10 μ Ci/ml; Perkin Elmer) was added in a methionine- and cysteine-free medium for 3 h. Cell extracts were prepared in RIPA buffer and subjected to benzonase treatment (0.25 U/ μ l in presence of 7.5 mM MgCl₂ for 1 h at 4°C). After centrifugation, 4–6 mg lysates were employed in immunoprecipitation of EGFP-tagged p14^{ARF}. Immunoprecipitates were analyzed by SDS–PAGE followed either by immunoblotting or fluorography. For fluorography, gels were incubated with Enlight enhancing solution (Mo Bi Tec) and vacuum dried at 80°C. Radioactive signals were detected using X-ray films (Hyperfilm; Amersham) and intensifying screens (Kodak).

In vitro MT assays

In vitro methylation assays were performed in the presence of radiolabeled SAM (¹⁴C-labeled methyl-group) using recombinant GST-tagged substrates and PRMT enzymes purified from bacteria or eukaryotic cells as described in (Hyllus *et al*, 2007; Berberich *et al*, 2017). Eluted GST-tagged or Flag-tagged PRMT enzymes or immunoprecipitated HA-tagged PRMT5/Myc-tagged MEP50 were incubated with substrates (either bead-bound GST-tagged proteins or histone H3, H4, or bulk histones from calf thymus; Sigma-Aldrich) in the presence of [¹⁴C-methyl]-S-adenosyl-methionine (¹⁴C-methyl-SAM 20 μ Ci/ml; Perkin Elmer) for 1–2 h at 37°C. Reactions were separated by SDS–PAGE and blotted on PVDF membrane for autoradiography and subsequent immunostaining. Radioactive signals were detected using X-ray films (Hyperfilm; Amersham) and intensifying screens (Kodak).

Pull-down assays

Pull-down assays using bead-coupled peptides or GST-tagged proteins were performed as described in the Appendix Supplementary Methods. Unmodified and modified p14^{ARF} NLS/NoLS peptides followed by a C-terminal cysteine residue were obtained from Peptide Specialty Laboratories (Heidelberg, Germany).

Flow cytometry

For detection of cell cycle distribution and apoptosis/necrosis, flow cytometry was used as recently described in (Streubel *et al*, 2013; Bouchard *et al*, 2018). In detail, for quantification of cell cycle distribution, cells were harvested, washed in ice-cold PBS, and fixed in ice-cold 70% ethanol overnight. After complete permeabilization, cells were washed twice with FACS buffer. DNA was then stained with 54 μ M propidium iodide (PI, Sigma-Aldrich) in the presence of 38 mM sodium citrate and 250 μ g/ml RNase A for 30 min at 37°C in the dark. For quantification of phosphatidylserine on the surface of UVC-treated cells, $0.5\text{--}1 \times 10^6$ unfixed cells were incubated with FITC-labeled Annexin-V and/or PI (BD Pharmingen) according to the manufacturer's instructions. All samples were analyzed using BD FACSCalibur flow cytometer (BD Bioscience). Data were processed using the CellQuestPro or FlowJo (FlowJo LLC) Software.

Immunofluorescence (IF) stainings

Localization and expression levels of p14^{ARF} and PRMT1 were detected in cell lines and human pancreatic tissue of PDAC patients by immunofluorescence stainings (IF) and immunohistochemistry stainings (IHC). For IF stainings of cells, cells were grown on glass coverslips and fixed with either 4% formaldehyde at RT or methanol at -20°C for 10–15 min, permeabilized in PBS with 0.3% Triton X-100 for 5 min, and incubated with blocking solution (PBS; 0.1–0.3% Triton X-100 or without Triton X-100; 5% BSA) for 45–60 min. Incubation with primary antibodies (Appendix Supplementary Methods) was performed in blocking solution at RT for 2 h. Cells were washed three times in PBS, followed by incubation with fluorophore-linked secondary antibodies (Appendix Supplementary Methods) for 30–75 min. Subsequently, cells were stained with DAPI (0.15 mg/ml; Sigma-Aldrich) in PBS for 2–4 min, washed three times in PBS, once in water, and then embedded in mounting medium (Mowiol4-88 with DABCO, Roth). Stainings were analyzed using a Leica DMR fluorescence microscope and the Confocal Laser Scanning microscope Leica SP8i, followed by analysis with the Leica LAS AF and Fiji software. For quantification of subcellular p14^{ARF} localization, ≥ 200 cells per condition and biological replicate were counted and grouped into exclusively nucleolar, not-exclusively nucleolar but additionally/predominantly nucleolar/cytoplasmic or exclusively cytoplasmic localization.

For IF staining of human tissue, formalin-fixed and paraffin-embedded PDAC samples and corresponding normal pancreas were deparaffinized and hydrated as for IHC. For antigen retrieval, tissue sections were steam-heated for 35 min in citrate buffer (pH 6.0) and then washed in PBS. For reducing the background staining, sections were incubated twice 5 min in 100 mM glycine, followed by rinsing three times in TBS with 0.1% Tween (TBS-T) and incubation in blocking solution (PBS; 10% chicken serum; 0.3% Triton X-100) at RT for 60 min. Incubation with primary antibodies (Appendix Supplementary Methods) was performed overnight at 4°C in blocking solution with 5% chicken serum. Subsequently, the sections were washed three times with TBS-T and blocked for 30 min in blocking solution followed by incubation with secondary antibodies (Appendix Supplementary Methods) and DAPI (0.15 μ g/ml; Sigma-Aldrich) for 90 min at RT. After 3 additional washing steps in TBS-T and one washing step in water, the sections were embedded

in mounting medium (Mowiol4-88 with DABCO, Roth) and stored at 4°C. Fluorescence images were captured using the Confocal Laser Scanning microscope Leica SP8i and analyzed using the Leica LAS AF software.

Immunohistochemistry (IHC) stainings

Formalin-fixed and paraffin-embedded archived human PDAC samples and corresponding normal tissues were stained as follows. Tissue sections were heated to 60°C for 1 h, deparaffinized using xylene, and hydrated by a graded series of ethanol washes. Antigen retrieval was accomplished by steam-heating in target retrieval solution (pH 9.0, Dako) for 30 min. Endogenous peroxidase activity was quenched by 5-min incubation in 3% H₂O₂. Sections were then incubated with primary antibodies (Appendix Supplementary Methods) for 45 min at RT followed by biotinylated secondary antibodies for 20 min also at RT. Bound antibodies were detected using the avidin–biotin complex (ABC) peroxidase method (ABC Elite Kit; Vector Labs, Burlingame, California, USA). Final staining was developed with the Dako DAB peroxidase substrate kit. For double staining, HRP Magenta Substrate Chromogen System was employed. Counterstaining was performed using hematoxylin. All steps following the antigen retrieval were performed using the DakoCytomation Autostainer Plus. The quantitation of PRMT1 positive cells was performed using the virtual software programs Fiji ImageJ (Schindelin *et al*, 2009) and ViewPoint software version 2018-02-05 from PreciPoint GmbH (Freising, Germany). Quantitative expression scores for PRMT1 were determined by counting of ≥ 100 tumor cells per specimen. Scores (not elevated, moderately elevated or highly elevated PRMT1 expression) are based on the immunostaining intensity and the percentage of stained tumor cells in PDAC tissues compared to normal pancreas.

Protein and RNA isolation

Protein and RNA isolation for immunoblotting, immunoprecipitation, or reverse transcription quantitative PCR (RT–qPCR) was performed as described in the Appendix Supplementary Methods.

Statistical analysis

All experiments were performed at least three times (biological replicates, n-values as indicated in the figure legends) and are represented as mean \pm SD. Reproducible and representative data sets are shown. Corresponding statistical tests are mentioned in the figure legends.

Data availability

This study includes no data deposited in external repositories.

Expanded View for this article is available online.

Acknowledgements

We thank present and former members of the U.M.B. laboratory, in particular Kaatje Heinelt, Lara Kleinesudek, Dr. Anna-Lena Jung, Alessia Pantaleoni, Caroline Reuter, and Dr. Saleh Hassan Sharif Ahmed, for their active support during the work progress. We are grateful to Dr. Katrin Roth from Cellular Imaging

Unit for microscopy support, Dr. Annette Ramaswamy from the Department of Pathology for pancreas tissue evaluation, and Dr. Ina Petra Pfeifferle from the Comprehensive Biomaterial Bank for tissue archiving. Further, we thank Viktoria Wischmann, Inge Sprenger, and Silke Caspari for their excellent technical assistance. This work was funded by the DFG (Deutsche Forschungsgemeinschaft) to DKB and UMB as part of the KFO325 (BA 1467/6, BA 2292/5) and to UMB as part of TRR81 A03, SFB1213 A06, BA 2292/1, and BA 2292/4.

Author contributions

AR: Investigation, Validation, Formal Analysis, Visualization. DH: Investigation, Validation, Formal Analysis, Visualization, Writing—review and editing. CB: Investigation, Validation, Formal Analysis, Visualization, Writing—review and editing. MM: Investigation, Validation, Formal Analysis, Visualization, Writing—review and editing. YV-Y: Investigation. HR: Investigation, Formal Analysis. LH: Investigation. EKra: Investigation, Validation, Writing—review and editing. EKre: Resources. RF: Resources. CUK: Resources, Methodology. ML: Resources, Methodology, Writing—review and editing. EPS: Supervision, Writing—review and editing. DKB: Funding acquisition, Supervision, Writing—review and editing. U-MB: Project Administration, Funding acquisition, Conceptualization, Supervision, Formal Analysis, Visualization, Writing—original draft.

Conflict of interest

The authors declare that they have no conflict of interest.

References

- Anaya J (2016) OncoLnc: linking TCGA survival data to mRNAs, miRNAs, and lncRNAs. *PeerJ Comput Sci* 2: e67
- Ayrault O, Olivier A, Karayan L, Lucie K, Riou J-F, Jean-François R, Larsen C-J, Christian-Jacques L, Séité P, Paule S (2003) Delineation of the domains required for physical and functional interaction of p14ARF with human topoisomerase I. *Oncogene* 22: 1945–1954
- Bao X, Siprashvili Z, Zarnegar BJ, Shenoy RM, Rios EJ, Nady N, Qu K, Mah A, Webster DE, Rubin AJ et al (2017) CSNK1a1 regulates PRMT1 to maintain the progenitor state in self-renewing somatic tissue. *Dev Cell* 43: 227–239
- Berberich H, Terwesten F, Rakow S, Sahu P, Bouchard C, Meixner M, Philipson S, Kolb P, Bauer U-M (2017) Identification and in silico structural analysis of Gallus gallus protein arginine methyltransferase 4 (PRMT4). *FEBS Open Bio* 7: 1909–1923
- Blanc RS, Vogel G, Li X, Yu Z, Li S, Richard S (2017) Arginine methylation by PRMT1 regulates muscle stem cell fate. *Molecular Cell Biol* 37: e00457-16
- Boisvert FM, Dery U, Masson JY, Richard S (2005a) Arginine methylation of MRE11 by PRMT1 is required for DNA damage checkpoint control. *Genes Dev* 19: 671–676
- Boisvert FM, Rhie A, Richard S, Doherty AJ (2005b) The GAR motif of 53BP1 is arginine methylated by PRMT1 and is necessary for 53BP1 DNA binding activity. *Cell Cycle* 4: 1834–1841
- Bouchard C, Sahu P, Meixner M, Nötzold RR, Rust MB, Kremmer E, Feederle R, Hart-Smith G, Finkernagel F, Bartkuhn M et al (2018) Genomic location of PRMT6-Dependent H3R2 methylation is linked to the transcriptional outcome of associated genes. *Cell Rep* 24: 3339–3352
- Chen D, Kon N, Zhong J, Zhang P, Yu L, Gu W (2013) Differential effects on ARF stability by normal versus oncogenic levels of c-Myc expression. *Mol Cell* 51: 46–56
- Chen D, Shan J, Zhu W-G, Qin J, Gu W (2010) Transcription-independent ARF regulation in oncogenic stress-mediated p53 responses. *Nature* 464: 624–627
- Cheung N, Chan LC, Thompson A, Cleary ML, So CW (2007) Protein arginine-methyltransferase-dependent oncogenesis. *Nat Cell Biol* 9: 1208–1215
- Cheung N, Fung TK, Zeisig BB, Holmes K, Rane JK, Mowen KA, Finn MG, Lenhard B, Chan LC, So CW (2016) Targeting aberrant epigenetic networks mediated by PRMT1 and KDM4C in acute myeloid leukemia. *Cancer Cell* 29: 32–48
- Deer EL, González-Hernández J, Coursen JD, Shea JE, Ngatia J, Scaife CL, Firpo MA, Mulvihill SJ (2010) Phenotype and genotype of pancreatic cancer cell lines. *Pancreas* 39: 425–435
- Eram MS, Shen Y, Szewczyk MM, Wu H, Senisterra G, Li F, Butler KV, Kaniskan HÜ, Speed BA, Dela Seña C et al (2016) A Potent, Selective, and cell-active inhibitor of human type I protein arginine methyltransferases. *ACS Chem Biol* 11: 772–781
- Eyrin B, Claverie P, Salon C, Leduc C, Col E, Brambilla E, Khochbin S, Gazzeri S (2006) p14ARF activates a Tip60-dependent and p53-independent ATM/ATR/CHK pathway in response to genotoxic stress. *Mol Cell Biol* 26: 4339–4350
- Favia A, Salvatori L, Nanni S, Iwamoto-Stohl LK, Valente S, Mai A, Scagnoli F, Fontanella RA, Totta P, Nasi S et al (2019) The Protein Arginine Methyltransferases 1 and 5 affect Myc properties in glioblastoma stem cells. *Sci Rep* 9: 1–13
- Gallagher SJ, Kefford RF, Rizos H (2006) The ARF tumour suppressor. *Int J Biochem Cell Biol* 38: 1637–1641
- Guccione E, Richard S (2019) The regulation, functions and clinical relevance of arginine methylation Nature reviews | Molecular cell Biology. *Nat Rev Mol Cell Biol* 20: 642–657
- Hezel AF, Kimmelman AC, Stanger BZ, Hezel AF, Kimmelman AC, Stanger BZ, Bardeesy N, Depinho RA (2006) Genetics and biology of pancreatic ductal adenocarcinoma Genetics and biology of pancreatic ductal adenocarcinoma. *Genes Dev* 20: 1218–1249
- Hyllus D, Stein C, Schnabel K, Schiltz E, Imhof A, Dou Y, Hsieh J, Bauer U-M (2007) PRMT6-mediated methylation of R2 in histone H3 antagonizes H3 K4 trimethylation. *Genes Dev* 21: 3369–3380
- Itahana K, Zhang Y (2008) Mitochondrial p32 is a critical mediator of ARF-induced apoptosis. *Cancer Cell* 13: 542–553
- Karayan L, Riou JF, Séité P, Migeon J, Cantereau A, Larsen CJ (2001) Human ARF protein interacts with topoisomerase I and stimulates its activity. *Oncogene* 20: 836–848
- Kim WY, Sharpless NE (2006) The regulation of INK4/ARF in cancer and aging. *Cell* 127: 265–275
- Ko A, Shin JY, Seo J, Lee KD, Lee EW, Lee MS, Lee HW, Choi IJ, Jeong JS, Chun KH et al (2012) Acceleration of gastric tumorigenesis through MKRN1-mediated posttranslational regulation of p14ARF. *J Natl Cancer Inst* 104: 1660–1672
- Korgaonkar C, Hagen J, Tompkins V, Frazier AA, Allamargot C, Quelle FW, Quelle DE (2005) Nucleophosmin (B23) Targets ARF to nucleoli and inhibits its function. *Mol Cell Biol* 25: 1258–1271
- Kuo ML, Den Besten W, Bertwistle D, Roussel MF, Sherr CJ (2004) N-terminal polyubiquitination and degradation of the Arf tumor suppressor. *Genes Dev* 18: 1862–1874
- Lee C, Smith BA, Bandyopadhyay K, Gjerset RA (2005) DNA damage disrupts the p14ARF-B23(nucleophosmin) interaction and triggers a transient subnuclear redistribution of p14ARF. *Cancer Res* 65: 9834–9842
- Liu Q, Dreyfuss G (1995) *In vivo* and *in vitro* arginine methylation of RNA-binding proteins. *Mol Cell Biol* 15: 2800–2808
- Montenegro MF, González-Guerrero R, Sánchez-del-Campo L, Piñero-Madrona A, Cabezas-Herrera J, Rodríguez-López JN (2020)

- PRMT1-dependent methylation of BRCA1 contributes to the epigenetic defense of breast cancer cells against ionizing radiation. *Sci Rep* 10: 13275–13288
- Moulin S, Llanos S, Kim SH, Peters G (2008) Binding to nucleophosmin determines the localization of human and chicken ARF but not its impact on p53. *Oncogene* 27: 2382–2389
- Musiani D, Giambrodo R, Massignani E, Ippolito MR, Maniaci M, Jammula S, Manganaro D, Cuomo A, Nicosia L, Pasini D et al (2020) PRMT1 is recruited via DNA-PK to chromatin where it sustains the senescence-associated secretory phenotype in response to Cisplatin. *Cell Rep* 30: 1208–1222
- Ozenne P, Eymin B, Brambilla E, Gazzeri S (2010) The ARF tumor suppressor: Structure, functions and status in cancer. *Int J Cancer* 127: 2239–2247
- Pawlak MR, Scherer CA, Chen J, Roshon MJ, Ruley HE (2000) Arginine N-methyltransferase 1 is required for early postimplantation mouse development, but cells deficient in the enzyme are viable. *Mol Cell Biol* 20: 4859–4869
- Rizos H, Darmanian AP, Mann GJ, Kefford RF (2000) Two arginine rich domains in the p14ARF tumour suppressor mediate nucleolar localization. *Oncogene* 19: 2978–2985
- Rodway H, Llanos S, Rowe J, Peters G (2004) Stability of nucleolar versus non-nucleolar forms of human p14 ARF. *Oncogene* 23: 6186–6192
- Rust HL, Subramanian V, West GM, Young DD, Schultz PG, Thompson PR (2014) Using unnatural amino acid mutagenesis to probe the regulation of PRMT1. *ACS Chem Biol* 9: 649–655
- Sakamaki JI, Daitoku H, Ueno K, Hagiwara A, Yamagata K, Fukamizu A (2011) Arginine methylation of BCL-2 antagonist of cell death (BAD) counteracts its phosphorylation and inactivation by Akt. *Proc Natl Acad Sci USA* 108: 6085–6090
- Schindelin J, Arganda-Carrera I, Frise E, Verena K, Mark L, Tobias P, Stephan P, Curtis R, Stephan S, Benjamin S et al (2009) Fiji - an Open platform for biological image analysis. *Nat Methods* 9: 676–682
- Sherr CJ (2006) Divorcing ARF and p53: an unsettled case. *Nat Rev Cancer* 6: 663–673
- Shia WJ, Okumura AJ, Yan M, Sarkeshik A, Lo MC, Matsuura S, Komeno Y, Zhao X, Nimer SD, Yates JR et al (2012) PRMT1 interacts with AML1-ETO to promote its transcriptional activation and progenitor cell proliferative potential. *Blood* 119: 4953–4962
- Song C, Chen T, He L, Ma N, Li J, Rong YF, Fang Y, Liu M, Xie D, Lou W (2020) PRMT1 promotes pancreatic cancer growth and predicts poor prognosis. *Cell Oncol* 43: 51–62
- Stott FJ, Bates S, James MC, McConnell BB, Starborg M, Brookes S, Palmero I, Ryan K, Hara E, Vousden KH et al (1998) The alternative product from the human CDKN2A locus, p14(ARF), participates in a regulatory feedback loop with p53 and MDM2. *EMBO J* 17: 5001–5014
- Streubel G, Bouchard C, Berberich H, Zeller MS, Teichmann S, Adamkiewicz J, Muller R, Klempnauer KH, Bauer UM (2013) PRMT4 is a novel coactivator of c-Myb-dependent transcription in haematopoietic cell lines. *PLoS Genet* 9: e1003343
- Tang J, Frankel A, Cook RJ, Kim S, Paik WK, Williams KR, Clarke S, Herschman HR (2000) PRMT1 is the predominant type I protein arginine methyltransferase in mammalian cells. *J Biol Chem* 275: 7723–7730
- Vadnais C, Chen R, Fraszczak J, Yu Z, Boulais J, Pinder J, Frank D, Khandanpour C, Hébert J, Dellaire G et al (2018) GFI1 facilitates efficient DNA repair by regulating PRMT1 dependent methylation of MRE11 and 53BP1. *Nat Commun* 9: 1–14
- Wang X, Zha M, Zhao X, Jiang P, Du W, Tam AYH, Mei Y, Wu M (2013) Siva1 inhibits p53 function by acting as an ARF E3 ubiquitin ligase. *Nat Commun* 4: 1551
- Wang Y, Hsu J-M, Kang Y, Wei Y, Lee P-C, Chang S-J, Hsu Y-H, Hsu JL, Wang H-L, Chang W-C et al (2016) Oncogenic functions of Gli in pancreatic adenocarcinoma are supported by its PRMT1-mediated methylation. *Cancer Res* 76: 7049–7058
- Yamagata K, Daitoku H, Takahashi Y, Namiki K, Hisatake K, Kako K, Mukai H, Kasuya Y, Fukamizu A (2008) Arginine methylation of FOXO transcription factors inhibits their phosphorylation by Akt. *Mol Cell* 32: 221–231
- Yang Y, Bedford MT (2013) Protein arginine methyltransferases and cancer. *Nat Rev Cancer* 13: 37–50
- Yoshimatsu M, Toyokawa G, Hayami S, Unoki M, Tsunoda T, Field HI, Kelly JD, Neal DE, Maehara Y, Ponder BA et al (2011) Dysregulation of PRMT1 and PRMT6, Type I arginine methyltransferases, is involved in various types of human cancers. *Int J Cancer* 128: 562–573
- Yu Z, Chen T, Hebert J, Li E, Richard S (2009) A mouse PRMT1 null allele defines an essential role for arginine methylation in genome maintenance and cell proliferation. *Mol Cell Biol* 29: 2982–2996
- Zhang Y, Xiong Y (1999) Mutations in human ARF exon 2 disrupt its nucleolar localization and impair its ability to block nuclear export of MDM2 and p53. *Mol Cell* 3: 579–591
- Zhao X, Jankovic V, Gural A, Huang G, Pardanani A, Menendez S, Zhang J, Dunne R, Xiao A, Erdjument-Bromage H et al (2008) Methylation of RUNX1 by PRMT1 abrogates SIN3A binding and potentiates its transcriptional activity. *Genes Dev* 22: 640–653
- Zheng S, Moehlenbrink J, Lu YC, Zalmas LP, Sagum CA, Carr S, McGouran JF, Alexander L, Fedorov O, Munro S et al (2013) Arginine methylation-dependent reader-writer interplay governs growth control by E2F-1. *Mol Cell* 52: 37–51



License: This is an open access article under the terms of the Creative Commons Attribution-NonCommercial-NoDerivs 4.0 License, which permits use and distribution in any medium, provided the original work is properly cited, the use is non-commercial and no modifications or adaptations are made.